The Aryl Hydrocarbon Receptor Controls IFNγ-Induced Immune Checkpoints PD-L1 and IDO via the JAK/STAT Pathway in Lung Adenocarcinoma[1]

Megan Snyder*, Zhongyan Wang[#], Brian Lara[#], Jocelyn Fimbres[#],

Tachira Pichardo[##], Sarah Mazzilli[##], Mohammed Muzamil Khan[&],

Vinay K. Duggineni[#], Stefano Monti[&], David H. Sherr[#]

*Graduate Program in Genetics and Genomics, Boston University School of Medicine

#Department of Environmental Health, Boston University School of Public Health

&Section of Computational Biomedicine, Boston University Chobanian & Avedisian School of Medicine

Running Title: The AhR controls IFNγ Signaling and Immune Checkpoints

Corresponding author: David H. Sherr, Department of Environmental Health, Boston University School of Public Health, Boston, MA, USA. 02118; 617-358-1708, dsherr@bu.edu

Keywords: Aryl Hydrocarbon Receptor, Cancer, Tumor Immunity, Interferon Gamma

Abstract

While immunotherapy has shown efficacy in lung adenocarcinoma (LUAD) patients, many respond only partially or not at all. One limitation in improving outcomes is the lack of a complete understanding of immune checkpoint regulation. Here, we investigated a possible link between an environmental chemical receptor implicated in lung cancer and immune regulation, (the aryl hydrocarbon receptor/AhR), a known but counterintuitive mediator of immunosuppression (IFNγ), and regulation of two immune checkpoints (PD-L1 and IDO). AhR gene-edited LUAD cell lines, a syngeneic LUAD mouse model, bulk- and scRNA sequencing of LUADs and tumor-infiltrating leukocytes were used to map out a signaling pathway leading from IFNγ through the AhR to JAK/STAT, PD-L1, IDO, and tumor-mediated immunosuppression. The data demonstrate that: **1)** IFNγ activation of the JAK/STAT pathway leading to PD-L1 and IDO1 upregulation is mediated by the AhR in murine and human LUAD cells, **2)** AhR-driven IDO1 induction results in the production of Kynurenine (Kyn), an AhR ligand, which likely mediates an AhR→IDO1→Kyn→AhR amplification loop, **3)** transplantation of AhR-knockout LUAD cells results in long-term tumor immunity in most recipients. **4)** The 23% of AhR-knockout tumors that do grow do so at a much slower pace than controls and exhibit higher densities of CD8$^+$ T cells expressing markers of immunocompetence, increased activity, and increased cell-cell communication. The data definitively link the AhR to IFNγ-induced JAK/STAT pathway and immune checkpoint-mediated immunosuppression and support the targeting of the AhR in the context of LUAD.

Introduction

Lung cancer is one of the most commonly diagnosed and deadliest of human malignancies (1). More than half of all lung cancers are adenocarcinomas (LUAD), a subset of non-small cell lung cancers (NSCLCs) likely derived from alveolar type 2 cells (2). Smoking is the single greatest LUAD risk factor. However, LUAD is also the most common form of lung cancer seen in never-smokers (3). Surgery, radiotherapy, and chemotherapy remain front-line treatments for LUAD, with varying degrees of success. More recently, immunotherapy, particularly with monoclonal antibodies targeting the PD-1/PD-L1 axis either as monotherapy or in combination with traditional treatments, has proven effective in subsets of LUAD patients (4, 5). However, the proportion of patients eligible for immunotherapy remains limited and many patients respond only partially or not at all. Importantly, not all factors controlling expression of the immune checkpoints targeted by immunotherapy have been defined. That said, it has been shown that IFNγ, usually associated with positive immune responses, can contribute to immune suppression by upregulating PD-L1 and the indoleamine-2,3-dioxygenases, IDO1 and IDO2, proximal and redundant rate-limiting enzymes in the kynurenine (Kyn) pathway of tryptophan metabolism (6). Kyn itself, produced by IDO^+ melanomas (7), ovarian (8) (9), squamous cell (10), and colon (11) carcinomas induces potent immunosuppression in the tumor microenvironment (TME). At least one pathway through which IFNγ induces these immune checkpoints is the JAK/STAT pathway (12, 13). Therefore, it is important to identify factors that regulate the IFN-activated JAK/STAT pathway and lead to immune checkpoint expression and tumor-mediated immunosuppression. As shown herein, one such factor is the AhR.

The AhR is a ligand-activated transcription factor and protein-binding partner originally recognized for its activation by environmental chemicals including 2,3,7,8-tetrachlorodibenzo-p-

3

72   dioxin (TCDD), polychlorinated biphenyls (PCBs), and planar polycyclic aromatic hydrocarbons

73   (PAH). AhR activation induces expression of CYP1A1, CYP1A2, and CYP1B1 monoxygenases

74   capable of metabolizing some environmental AhR ligands, including PAH common in cigarette

75   smoke, into mutagenic intermediates (14). These smoke-derived mutagens have long been

76   associated with LUAD and other cancers (15, 16). Furthermore, and more germane to the present

77   studies, many of these same environmental AhR ligands are highly immunosuppressive (17, 18)

78   and the AhR itself, however it is activated, is associated with immunosuppression in several

79   contexts (19-23).

80   The effects of environmental chemicals aside, accumulating evidence implicates the AhR

81   in cancer even in the absence of environmental ligands (6, 24-26). Thus, the AhR is hyper-

82   expressed and chronically active in several cancers (27). It is now apparent that endogenous AhR

83   agonists are at least partially responsible for this activity and that they drive malignant cell

84   migration, metastasis, and cancer stem cell properties (28-31). Indeed, the level of AhR activity

85   is inversely related to survival in lung cancer patients (32). While AhR ligands may derive from

86   multiple sources, including the diet and microbiome (33, 34), some endogenous ligands originate

87   from within the TME itself (6, 27). One source of such agonists is the IDO-dependent Kyn

88   pathway of tryptophan metabolism. Notably, the AhR can upregulate expression of IDO1/2

89   which generates AhR ligands, including Kyn itself, through the Kyn metabolic pathway. Kyn-

90   activated AhR also has been implicated in PD-1 expression on tumor infiltrating T cells (7), and

91   on PD-L1 expression on primary human lung epithelial cells (35) and oral squamous cell

92   carcinomas (36).

93   The apparent influence of IFNγ and the AhR on IDO levels, Kyn production, and

94   immune checkpoint expression suggests the existence of an intricate pathway of interactions

4

95   involving IFNγ, AhR, IDO, Kyn (or its downstream metabolites/AhR ligands), and PD-L1

96   resulting in suppression of tumor immunity in the TME. Here, these interactions were more

97   clearly mapped using *AhR* knockout murine (CMT167) human (A549) LUAD cells, a syngeneic

98   LUAD mouse model, immunophenotyping, and bulk and single cell RNA sequencing of whole

99   LUAD and sorted tumor-infiltrating leukocytes respectively. Surprisingly, the results indicate a

100   novel pathway within LUAD cells in which the AhR controls IFN type II-induced JAK/STAT

101   signaling leading to IDO1/2 and PD-L1/PD-L2 expression and, ultimately, immunosuppression

102   in the TME. Collectively, the results reveal the AhR to be a master regulator of IFNγ signaling

103   and help explain mechanisms of immune checkpoint regulation, including the counterintuitive

104   role that IFN plays in immunosuppression in the LUAD context.

Materials and Methods

Cell lines and Cell Culture

Murine CMT167 lung adenocarcinoma cell line ("CMT167") were kindly provided by Dr. Raphael Nemenoff (University of Colorado-Denver). CMT167 cells were selected since they have commonly been used to study immune checkpoints in LUAD and since they harbor a KrasG12V mutation, one of the most common driver mutations in human NSCLC (37). Human A549 LUAD cells were obtained from the American Type Culture Collection (ATCC). The A549 cell line was chosen in part because it harbors a KrasG12S mutation, another common driver mutation in human LUADs, and because it has been used extensively to study regulation of immune checkpoints (38, 39). Cells were cultured in Dulbecco's Modified Eagle Medium (Corning Inc., Corning, NY) supplemented with 10% fetal bovine serum (Gemini Bioproducts LLC, West Sacramento, CA), 1% penicillin/streptomycin (Life Technologies, Gaithersburg, MD), and 1% L-glutamine (Fisher Scientific, Hampton, NH) at 37°C with 5% carbon dioxide. Cells were kept in culture no longer than eight weeks and new aliquots were thawed periodically. Cultures were confirmed to be mycoplasma negative every two months.

For *in vitro* RT-qPCR, western immunoblotting, and immunophenotyping experiments CMT167 or A549 cell lines (50,000 cells/well) were cultured in 6-or 12-well plates for 24-72 hours with or without 1-100 ng/ml IFNγ (PeproTech, Cranbury, NJ), 10 µM benzo(a)pyrene (B(a)P)(Sigma-Aldrich, Burlington, MA), or 0.5 µM 6-formylindolo(3,2-b)carbazole (FICZ)(Sigma-Aldrich, Burlington, MA). Each experiment included a minimum of three replicates, with each replicate representing a pool of at least two wells.

CRISPR/Cas9-mediated knockouts.

128   Single-guide RNAs (sgRNAs) targeting the mouse *AhR* gene (Exon1), the mouse *Ifnγr1*

129   gene (Exon1) and the mouse *Cd274 gene* (Exon1) were designed using the web resource

130   (https://www.synthego.com/products/bioinformatics/crispr-design-tool). Two individual sgRNAs

131   were used to target the *AhR* gene (sgRNA1, 5′-CGGCTTGCGCCGCTTGCGGC -3′; sgRNA2,

132   5′- AAACGTGAGTGACGGCGGGC-3′).. Complementary oligonucleotides for sgRNAs were

133   annealed, and cloned into the sgOpti vector (Addgene, Cambridge, MA, #85681) *BsmBI* sites

134   (40) using standard procedures (40). Lentivirus particles were generated in the HEK293NT cells

135   by co-transfecting the lentiCas9-Blast (Addgene, #52962), AhR-sgOpti, Ifnγr1-sgOpti or Cd274-

136   sgOpti plasmids, and the packaging plasmids (pLenti-P2A and pLenti-P2B, Cat. # LV003,

137   Applied Biological Materials Inc. Richmond, BC, Canada), using lipofectamine 2000

138   (Invitrogen) according to the manufacturer's instructions. Lentiviral particle-containing

139   supernatants were collected 24 and 48h after transfection and filtered using a 0.45-μm filter.

140   CMT167 cells were transduced with the lentivirus in the presence of 5 μg/ml polybrene. Forty-

141   eight hours after transduction, cells were selected with Blasticidin (5 μg/ml) and Puromycin (4

142   μg/ml) for two weeks. Gene deletion was validated by DNA sequencing (not shown), western

143   immunoblotting (**Supplemental Fig. 1A,D**) and by lack of transcriptional responsiveness (i.e.,

144   *CYP1B1* induction) in response to a strong AhR ligand (**Supplemental Fig. 1B,E**). Two AhR

145   knockout CMT167 clones, C1 and D2 (CMT167^{AhR-KO}), and two AhR knockout A549 clones,

146   P15 and P16 (A549^{AhR-KO}), were identified. Control lines (CMT167^{Cas9}) were generated with the

147   Cas9 vector without guide RNA.

148

149   **Colorimetric kynurenine assay**

7

150   Culture supernatants (160 µl) were transferred to 96-well round-bottom plates and mixed

151   with 10 µl / well 30% (v/v) freshly prepared trichloroacetic acid. The plates were incubated at

152   50°C for 30 minutes to hydrolyze N-formyl-kynurenine to kynurenine. Samples were centrifuged

153   at 3,000 g for 10 min. Aliquots of the supernatant (100 ml) were transferred to flat-bottom 96-

154   well plates and mixed with 100 µl freshly prepared Ehrlich's reagent (1.2% w/v 4-

155   dimethylamino-benzaldehyde in glacial acetic acid). Absorbance at 492 nm was measured using

156   a microplate reader (BioTek, Winooski, VT, USA) with the Gen5 software (BioTek) after a

157   10 min incubation. Kynurenine concentrations were calculated by reference to a standard

158   kynurenine curve.

159

160   RNA extraction and bulk RNA sequencing

161   CMT167^{AhR-KO}, A549^{AhR-KO}, wildtype (CMT167^{WT}) or CMT^{Cas9} cells, in triplicate or

162   quadruplicate wells, were harvested and total RNA was extracted using the RNeasy Plus Mini

163   Kit (QIAGEN, Hilden, Germany) according to the manufacturer's instructions. cDNA was

164   generated using the High-Capacity cDNA Reverse Transcription Kit (Applied Biosystems,

165   Waltham, MA) following the manufacturer's instructions. cDNA was sequenced using the

166   Boston University Microarray and Sequencing Core Facility. Between 18 and 28 million total

167   read pairs (CMT167 lines) or 50 to 71 million total read pairs (A549 lines) were obtained per

168   sample. Quality metrics were similar across all samples with no technical outliers. The Broad

169   Institute's Morpheus software (https://software.broadinstitute.org/morpheus, Broad Institute,

170   Cambridge, MA) was used to generate heat maps. QIAGEN's Ingenuity Pathway Analysis (IPA)

171   software https://qiagenbioinformatics.com/products/ingenuity-pathway-analysis, QIAGEN, Inc.)

172   was used to perform regulation pathway analyses.

8

173

RT-qPCR

Reverse Transcription-quantitative polymerase chain reaction (RT-qPCR) analysis was conducted with the QuantStudio 3 Real-Time PCR System (Thermo Fisher Scientific, Waltham, MA). Relative mRNA expression was quantified using the comparative Ct (ΔΔCt) method according to the ABI manual (Applied Biosystems). Amplification of glyceraldehyde-3-phosphate dehydrogenase (*Gapdh*) served as an internal reference in each reaction. Assays were performed in triplicate. The following TaqMan assays were purchased from Thermo Fisher Scientific: *Cd274* (Mm03048248_m1), *Ido1* (Mm00492590_m1), *Ido2* (Mm00524210_m1), *Cyp 1a1* (Mm00487218_m1), *Cyp1b1* (Mm00487229_m1), *Jak2* (Mm01208489_m1), *Stat1* (Mm012 57286_m1), *gapdh* (Mm99999915_g1), *CD274* (Hs00204257_m1), *IDO1* (Hs00984148_m1), *J AK2* (Hs01078136_m1), *STAT1* Hs01013996_m1), *STAT3(*Hs00374280_m1), *Muc1* (Mm00449604_m1), *Col5a1* (Mm00489299_m1), *Thbs1* (Mm01335418_m1), *Egfr* (Mm01187858_m1), *Itgb2* (Mm00434513_m1), *Cd109* (Mm00462151_m1), *Ccl2* (Mm00441242_m1), *Ccl5* (Mm01302427_m1),*GAPDH* (Hs99999905_m1).

Western blotting

Cells were grown to 70-80% confluence, harvested with trypsin, and lysed with radioimmunoprecipitation assay (RIPA) buffer with protease inhibitors. Blots were incubated overnight with AhR- (1:1000, #MA1-514, Thermo Fisher Scientific), PD-L1- (1:1000, ab213480, Abcam), or IDO1- (1:1000, #51851, Cell Signaling) specific antibodies and with β-actin- (1:2000, # A5441, Sigma-Aldrich) or GAPDH- (1:1000, #97166, Cell Signaling) specific antibody to serve as a loading control.

***In vivo* experiments**

196   Six to eight week-old C57BL/6J mice (Jackson Laboratories) were anesthetized and the

197   right flank injected subcutaneously with CMT167^{WT} or CMT167^{AhR-KO} cells using a 1 ml syringe

198   and 27½ gauge needle with 10^6 cells in Hank's Balanced Salt Solution. The *in vitro* growth rates

199   of CMT167^{AhR-KO} clones C1 and D2 and A549^{AhR-KO} clones P15 and P16 and their respective

200   WT and Cas9 controls were not significantly different. Average tumor size per mouse was

201   determined using a caliper and tumor volume calculated as (width^2 x length)/2. Tumors were

202   excised by cutting the surrounding fascia with scissors to separate the largely round tumor tissue

203   suspended between the dermis and peritoneum. For rechallenge experiments, 10^6 CMT167^{WT}

204   cells were injected into the left flank 65 days after a previous injection of CMT167^{AhR-KO} cells

205   into the right flank. Euthanasia was performed when one dimension of the tumor reached 20 mm

206   or when ulceration without fibrin crust formation was seen.

207   .

208   **Tumor infiltrating leukocyte (TIL) isolation**

209   Single cell suspensions of tumor-infiltrating leukocytes were obtained by chopping and

210   digesting tumors in 1.25 mg/mL collagenase IV (STEMCELL Technologies, Cambridge, MA),

211   0.025 mg/mL hyaluronidase (Sigma-Aldrich), and 0.01 mg/mL DNAse I (Sigma-Aldrich)

212   followed by washing in HBSS and processing using the Miltenyi GentleMACS system

213   (Miltenyi, Bergisch Gladbach, Germany). Digests were then filtered using 70 µm cell strainers.

214   For some experiments, (e.g., single cell RNA sequencing, intracellular cytokine staining) digests

215   were further cleaned by magnet bead separation of dead cells from live cells using Miltenyi's

216   Dead Cell Removal Kit per manufacturer's instructions.

217

218   **Flow cytometry**

219   Live cells in single cell suspensions were identified using a Fixable Live/Dead stain

220   (Biolegend, San Diego, California) followed by staining according to the manufacturer's

221   protocol. For intracellular markers, cells were first fixed and permeabilized (eBioscience,

222   Waltham, MA). All antibodies were purchased from Biolegend or Thermo Fisher Scientific

223   except for the unconjugated anti-L-kynurenine antibody which was obtained from ImmuSmol

224   (Bordeaux, France). All surface markers were stained at concentrations between 1:50 to 1:200,

225   and all intracellular markers were stained at a concentration of 1:100 to 1:200. L-kynurenine

226   staining required a secondary antibody which was used at a 1:100 concentration. Assays were

227   analyzed using the Cytek Aurora flow cytometer (Cytek Biosciences, Freemont, CA).

228   Representative CD4, CD8, CD44, and PD1 plots are provided in **Supplemental Figure 2**.

229

230   **Immunofluorescence**

231   Subcutaneous lung adenocarcinomas and whole lungs were fixed in 10% neutral buffered

232   formalin for 24-48h, processed and embedded in paraffin before being cut into 5 μm sections.

233   Mounted slides were used immediately or stored at -80^0 C to preserve antigens for

234   immunofluorescence. Formalin fixed, paraffin embedded sections were deparaffinized in xylene

235   baths followed by ethanol bath rehydration. Antigen retrieval was performed in pH 10 Tris-HCL

236   buffer (Sigma-Aldrich) by microwaving samples for 10 min at 20% power. Samples were then

237   blocked for 1 hour in 5% goat serum and PBS and then incubated overnight at 4° C with CD45-

238   specific (Abcam, Cat# ab154885, 1:100) or AhR-specific (Abcam Cat# ab213480, 1:50)

239   primary antibodies in blocking buffer. After washing in PBS + 0.1% Tween20 (PBST),

240   AlexaFluor® 488-labelled secondary antibody (AbcamA27034, 1:400) was added and samples

241   were incubated for 1 hour in blocking buffer. After washing with PBST, slides were sealed with

242   DAPI Prolong Gold, dried and imaged within two days on a Zeiss Axioscan.Z1 Slide Scanner.

243   Fluorescent quantification was done by selecting the whole tissue sections, detecting cells from

244   the DAPI channel and loading antibody channel classifiers in QuPath.

245

246   **Single Cell RNA sequencing (scRNA-seq) and analysis**

247   CMT167^{WT} or CMT167^{AhR-KO} tumors were digested as above and dead cells removed by

248   magnetic bead separation using Miltenyi's Dead Cell Removal Kit. Single cell suspensions were

249   sorted for live CD45$^+$ cells and resuspended in 0.04% BSA (Sigma). Viability was determined

250   manually by trypan blue exclusion and cells were shown to be $\geq$90% viable. An average of 5,792

251   viable cells from wildtype tumors and an average of 3,173 viable cells from AhR-KO tumors

252   were loaded into an Illumina cartridge in the Boston University Microarray and Single Cell

253   Sequencing Core Facility. Barcoding and scRNA-seq cDNA library preparation were done using

254   the Chromium platform from 10X Genomics in accordance with the manufacturer's guide.

255   Sequencing was done using the Illumina NexSeq2000 System. Over 150 million reads were

256   obtained per sample.

257   Single cells were preprocessed using singlecellTK (41) by applying doublet detection

258   (aggregation of four methods; scDblFinder, cxds, bcds, doubletFinder), decontamination (5%),

259   and filtering for mitochondrial gene content (>20%). Low cell-gene content was filtered (<400

260   genes per cell). SingleR (42) using the ImmGen compendium (43) identified cell types unique to

261   the immune repertoire and T cells were filtered for this analysis. Seurat R package (44) was used

262   for clustering and differential expression analysis. CD4$^+$/CD8$^+$ classification was performed

263   using gene expression level of markers (*CD4* or *CD8A*) with a cutoff > 60%. CellChat was used

12

264 to evaluate the number and relative strengths of interactions between T cells and antigen

265 presenting cells (45).

266 Geneset variation analysis (GSVA) (46) was applied to SCT-transformed counts against

267 an updated reference gene panel generated from LM22 hematopoietic cells (47). GSVA scores

268 were obtained for each cell and the sub-type with the maximum value for each cell was classified

269 as that sub-type. Differential gene expression (DGE) analysis was carried out via the Model-

270 based Analysis of Single-cell Transcriptomics (MAST) wrapper (48) in Seurat. DGE was applied

271 to clusters specific to either CD4 or CD8 cell-types in a one-vs-all approach and the $\log_{FC}$ and p-

272 value ≤ 0.05 were reported.

273 Gene Set Enrichment Analysis (GSEA) was performed using the clusterProfiler package

274 to assess enrichment in differentially expressed genes (DEGs) from published and curated

275 immunologic signature gene sets in MSigDB. Parameters were set to include a minimum of 25%

276 expressing cells and a minimum average log2 fold change of 0.25. The FindMarkers function in

277 Seurat, with the MAST wrapper, was used to rank DEGs by decreasing average log2 fold change

278 (-log2FC) and adjusted p-value (-log10). The ranked genes were then input into the GSEA

279 enrichment function using the ImmuneSigDB gene sets from the MSigDB website.

280

281 **Statistical Analyses**

282 Statistical tests (Student's t-test, ANOVA, Non-linear curve fit, Kaplan-Meier test) are

283 indicated in the figure legends. Graphing and statistical analyses were performed in Prism

284 (GraphPad). P or FDR values of <0.05 were considered significant, and error bars represent

285 standard error of the mean (SE). The Broad Institute's Morpheus software was used to generate

286 heat maps (https://software.broadinstitute.org/morpheus, Broad Institute, Cambridge, MA).

Results

Genome-wide analysis of AhR-regulated genes in murine and human LUAD cells.

To generate a global transcriptomic profile of AhR-regulated genes in LUAD cells, the AhR was deleted from murine CMT167 (CMT167^{AhR-KO}) and human A549 (A549^{AhR-KO}) cells by CRISPR/Cas9 gene editing. Controls were transduced with the Cas9-containing vector without guide RNA (CMT167^{Cas9}). AhR knockout in two CMT167 clones, D2 and C1, and A549 clones, P15 and P16, was confirmed by western blotting and by failure of a strong AhR ligand, 6-formylindolo(3,2-b)carbazole (FICZ), to induce *CYP1B1*, a canonical AhR-driven gene (**Supplementary Fig. 1A,B,D,E**). Lentivirus transduction had no effect on the *in vitro* growth of AhR-KO lines (**Supplementary Fig. 1C,F**). Bulk RNA sequencing of CMT167^{Cas9} and CMT167^{AhR-KO} cells demonstrated that 883 genes were significantly downregulated ($\geq$2-fold, FDR<0.05) and 756 genes were significantly upregulated ($\geq$2-fold, FDR<0.05) in both CMT167^{AhR-KO} and A549^{AhR-KO} cells. (The complete list of differentially expressed genes in both lines can be found at GEO accession GSE241980). As expected, expression of the AhR-driven *CYP1A1* and *CYP1B1* genes decreased significantly after AhR knockout in both cell lines (**Fig. 1A,B**).

Included in the set of downregulated genes in both lines were five genes previously shown to be important in LUAD but not commonly associated with the AhR, i.e., *MUC1* (49), *COL5A1* (50), *THBS1* (51), *EGFR* (52), and *ITGβ2* (53) (**Fig. 1A,B**). Of particular note, *ITGβ2* expression on malignant cells is associated with myeloid-derived suppressor cell infiltration in LUAD (54). Six additional genes associated with immune regulation in LUAD, *CD109* (55), *CCL2* (56), *CCL5* (57), *IDO1, IDO2* (58), and *CD274 (PD-L1)* (59), were significantly

309   downregulated in one or both cell lines. Down-regulation of *Muc1*, *Col5a1*, *Thbs1*, *Egfr*, *Cd109*,

310   *Ccl2* and *Ccl5* in CMT167[AhR-KO] cells was confirmed by RT-qPCR (**Fig. 2**).

311   The apparent down-regulation of *IDO1 and IDO2* in LUAD cells, as seen by RNA-seq,

312   was consistent with our studies and those of others demonstrating that the AhR regulates IDO1

313   or IDO2 in breast cancer (27, 60, 61) and dendritic cells (62, 63). Similarly, the down-regulation

314   of *CD274* after AhR knockout is consistent with data showing a correlation between AhR and

315   PD-L1 expression in LUAD patients (35)**.** Given the critical role of IDO1, IDO2 and CD274 in

316   suppression of tumor-specific responses, we then sought to confirm AhR control of these genes

317   in LUAD cells and to assess the relationship of the AhR to other signaling pathways, specifically

318   the IFNγ-induced JAK/STAT pathway, known to influence expression of these immune

319   checkpoints.

320

AhR regulates PD-L1 and IDO expression in CMT167 cells.

322   While not yet shown to be effective as monotherapies (64), IDO inhibitors are still in

323   clinical trials for treatment of LUAD, generally in combination with PD-1/PD-L1 blockade (65-

324   67). Given the importance of these mediators of immune suppression and the RNA-seq results

325   suggesting AhR control of *IDO* and *CD274*, we then sought to confirm AhR regulation of *Ido1,*

326   *Ido2* and *Cd274* in CMT167 cells. RT-qPCR analysis confirmed significant decreases in baseline

327   levels of *Cd274*, *Ido1*, *Ido2*, and, as positive controls, *Cyp1a1*, and *Cyp1b1*, in CMT167[AhR-KO]

328   cells as compared with control cells (**Fig. 3A, first two bars in each plot**). (*Tdo2* expression was

329   below the level of detection). These results suggest the presence of endogenous AhR ligand(s)

330   that drives baseline levels of these genes. Treatment with 10 μM of the environmentally common

331   smoke constituent and AhR agonist, benzo(a)pyrene (B(a)P), significantly increased expression

15

332   of all five genes in control cells and those increases were significantly muted or absent in

333   CMT167[AhR-KO] cells (**Fig. 3A, second two bars in each plot**).

334   Similarly, naïve CMT167[AhR-KO] cells expressed significantly less baseline PD-L1 protein

335   than control cells as seen by a representative western immunoblot (**Fig. 3B, left**) and by

336   quantification of β-actin-normalized band densities from three independent experiments (**Fig.**

337   **3B, right**). B(a)P increased PD-L1 protein levels and that increase was significantly muted in

338   CMT167[AhR-KO] cells (**Fig. 3B**). Consistent with AhR control of *Ido1 and Ido2* levels, B(a)P

339   increased baseline levels of Kyn in CMT167[WT] cells and that increase was significantly lower in

340   CMT167[AhR-KO] cells (**Fig. 3C**). These results demonstrate that both baseline and environmental

341   chemical-induced levels of two important immune checkpoints PD-L1 and IDO1/2, and a related

342   effector of immunosuppression, Kyn, are AhR controlled.

343

344   **IFNγ-mediated induction of PD-L1, IDO1, JAK2, and STAT1 is partially regulated by the**

345   **AhR.**

346   Although most often associated with protective T cell immunity, IFNγ also can

347   upregulate PD-L1 (12, 13) and IDO (68) thereby suggesting the counterintuitive conclusion that

348   chronic production of IFNγ, presumably by TILs, may be counterproductive to the anti-tumor

349   immune response. To determine if the AhR plays a role in IFNγ-mediated induction of these

350   immune checkpoints in LUAD cells, control and CMT167[AhR-KO] cells were treated with IFNγ

351   and *Cd274*, *Ido1*, and *Ido2* mRNA quantified by RT-qPCR after 24 (*Cd274*) or 72 (*Ido1*, *Ido2*)

352   hours. *Cyp1a1* and *Cyp1b1* mRNA levels were measured as controls. As shown previously (**Fig.**

353   **3**), CMT167[AhR-KO] cells expressed significantly lower baseline levels of all five genes than

354   control cells (**Fig. 4A**, **first two bars in each plot**). In control cells, IFNγ induced about a 95-,

355   15,500-, and 60-fold increase in *Cd274*, *Ido1*, and *Ido2* expression, respectively (**Fig. 4A, third**

356   **bar**). However, IFNγ-mediated induction of all three genes was significantly muted in

357   CMT167^{AhR-KO} cells (**Fig. 4A, fourth bar**). As expected from the IFNγ-driven increase in *Ido1*

358   *and Ido2*, generators of tryptophan-derived AhR ligands, both *Cyp1a1* and *Cyp1b1* transcripts

359   increased in an AhR-dependent way (**Fig. 4A**). To our knowledge, this is the first demonstration,

360   in any context, of this critical T cell cytokine increasing these two AhR-driven metabolic gene

361   transcripts.

362   As expected from RT-qPCR results, IFNγ-mediated induction of PD-L1 (**Fig. 4B**) and

363   IDO1 (**Fig. 4C**) protein was significantly lower in CMT167^{AhR-KO} cells. (Note that IFNγ led to

364   such dramatic increases in PD-L1 and IDO1 protein that the exposure time in the Western blots

365   had to be shortened and, therefore, was insufficient for revealing baseline PD-L1 or IDO1

366   levels). Consistent with AhR-regulation of IFNγ-induction of IDO, increasing IFNγ doses

367   increased Kyn levels, as quantified by a Kyn-dependent colorimetric assay, in a dose-dependent

368   manner and that increase was reduced in CMT167^{AhR-KO} cells (p<0.0001) (**Fig. 4D**).

369   Previous studies demonstrated a role for the JAK/STAT signaling pathway in PD-L1

370   expression in lung cancer (69) and a correlation between JAK/STAT, IDO, and PD-L1 in other

371   cancers (70-72). The JAK/STAT pathway can be activated by IFNγ in various cancers including

372   LUAD (73). Therefore, a possible role for the AhR in regulating IFNγ-mediated upregulation of

373   *Jak* or *Stat* was evaluated. Baseline *Jak2* levels, as quantified by RT-qPCR, were lower in

374   CMT167^{AhR-KO} cells relative to controls (**Fig. 4E, left, first two bars**). IFNγ modestly but

375   significantly increased *Jak2* in control cells but not in CMT167^{AhR-KO} cells. No differences in

376   baseline *Stat1* levels were seen between control and CMT167^{AhR-KO} cells. However, IFNγ

377   increased *Stat1* levels by ~90-fold in control cells and this *Stat1* induction was significantly

17

378   reduced in CMT167[AhR-KO] cells (**Fig. 4E, right**) implicating the AhR in IFNγ induction of *Jak2*

379   and *Stat1*.

380   These studies were then extended to the human A549 LUAD line with similar, if not

381   more profound results. In A549 cells, AhR knockout significantly reduced baseline levels of

382   *CD274*, *IDO1,* and *CYP1B1* mRNAs (**Fig. 5A, first two bars in each graph**). (*IDO2* and

383   *CYP1A1* mRNAs in A549 cells were at or below the level of detectability). IFNγ significantly

384   increased expression of all three genes in control cells but that increase was significantly muted

385   or absent in A549[AhR-KO] cells (**Fig. 5A, second two bars**). As expected from the *CD274* RT-

386   qPCR results, the baseline percentages of PD-L1^{+} cells, as quantified by flow cytometry, were

387   significantly reduced in A549[AhR-KO] cells (**Fig. 5B, first two bars**). IFNγ increased the

388   percentage of PD-L1[+] A549[Ctrl] cells but not the percentage of PD-L1[+] A549[AhR-KO] cells (**Fig. 5B,**

389   **second two bars**).

390   As expected from the IFNγ-induced *IDO1* mRNA quantification (**Fig. 5A**), AhR

391   knockout significantly decreased the percentage of Kyn^{+} cells (**Fig. 5C**). Similarly, titered

392   concentrations (1-1000 ng/ml) of IFNγ significantly induced Kyn production in control cells, but

393   minimally if at all in A549[AhR-KO] cells (**Fig. 5D**).

394   Consistent with data obtained in murine CMT167 lines (**Fig. 4**), baseline *JAK2*, *STAT1,*

395   and *STAT3* mRNA levels were significantly lower in A549[AhR-KO] cells as compared with controls

396   (**Fig. 5E, first two bars**). IFNγ significantly increased *JAK2*, *STAT1*, and *STAT3* in control but

397   not in A549[AhR-KO] cells (**Fig. 5E, third and fourth bars**). IFNγ did not affect AhR levels in

398   either CMT167 or A549 cells (not shown).

399   Collectively, the data generated in murine CMT167 and human A549 LUAD cells

400   demonstrate that the AhR influences the baseline and IFNγ-induced expression of key immune

401   regulators, IDO and PD-L1, as well as components of the JAK/STAT signaling pathway that are

402   known to regulate PD-L1 and IDO expression.

403

404   **AhR deletion in CMT167 cells imparts partial immune protection *in vivo*.**

405   The lower levels of baseline and IFNγ-induced IDO1/2 and PD-L1 in CMT167^{AhR-KO}

406   cells suggest the potential for an enhanced immune response to these cells *in vivo*. To test this

407   hypothesis, growth of wildtype, Cas9 control and AhR-KO CMT167 clones C1 and D2 cells was

408   determined in syngeneic C57BL/6 mice. CMT167^{WT} and CMT^{Cas9} tumors emerged at

409   approximately day 14 in each of the 16 mice injected and grew rapidly over the next 10 days

410   (**Fig. 6A**). All of these mice required euthanasia by day 30 because of skin lesions over the tumor

411   cell injection site. In contrast, of the 64 mice injected with CMT167^{AhR-KO} clones C1 and D2, 49

412   (77%) failed to grow tumors by day 53 (**Fig. 6A, red arrow**). Of the CMT167^{AhR-KO} tumors that

413   did grow, they grew at a significantly slower pace than control tumors (**Fig. 6B**).

414   To determine if the slow/lack of growth of CMT167^{AhR-KO} tumors reflected a heightened

415   immune response to CMT167^{AhR-KO} cells as compared with controls, 20 of the mice that failed to

416   generate CMT167^{AhR-KO} tumors by day 53 were inoculated in the contralateral flank with

417   CMT167^{WT} cells. Ten age-matched naïve mice were injected with CMT167^{WT} cells as positive

418   controls. Of the 20 mice that had previously been inoculated with CMT167^{AhR-KO} cells, none

419   grew tumors at the original site of CMT167^{AhR-KO} cell inoculation within 40 days of the

420   rechallenge and 13 of the 20 (65%) never grew wildtype tumors in the contralateral flank (**Fig.**

421   **6C, red arrow**). The seven CMT167^{WT} tumors that did grow grew significantly more slowly

422   than CMT167^{WT} tumors generated in naïve controls (**Fig. 6D)**. These data indicate that AhR

423   deletion in CMT167 cells induces a systemic and relatively long-lasting immunity with the

424   potential for complete tumor clearance.

425

426   **AhR deletion in CMT167 cells enables tumor-infiltrating T cell recruitment.**

427   To characterize the nature of the immunity imparted by transplantation of AhR-knockout

428   CMT167 cells, CMT167^{WT} and CMT167^{AhR-KO} tumors were excised, formalin fixed and

429   sectioned five weeks after transplantation and evaluated by immunofluorescence for AhR

430   expression and infiltration of CD45$^+$ cells. While AhR$^+$ CMT167^{WT} tumors were nearly devoid

431   of immune cells, significant numbers of CD45$^+$ cells were seen in CMT167^{AhR-KO} tumors (**Fig.**

432   **7A**). When quantified, this translated to a ~5-fold higher density of CD45$^+$ cells/mm^3 in the

433   CMT167^{AhR-KO} tumors as compared with CMT167^{WT} cells (p<0.0001)(**Fig. 7B**).

434   Flow cytometric analysis of CD45$^+$ immune cells from tumors that were excised and

435   digested at two, three, four, and five weeks after transplantation revealed relatively few

436   CD45$^+$CD4$^+$ or CD45$^+$CD8$^+$ T cells in CMT167^{WT} tumors, resulting in a very low T cell density

437   at any time point (**Fig. 7C, black circles**). (Representative dot plots are provided in

438   **Supplemental Fig. 2**). In contrast, an increasing density of CD4$^+$ and CD8$^+$ T cells was noted

439   over time in CMT167^{AhR-KO} tumors (**Fig. 7C**, **red circles**). Indeed, the smaller CMT167^{AhR-KO}

440   tumors generally had a greater absolute number of infiltrating CD4$^+$ and CD8$^+$ T cells than the

441   larger CMT167^{WT} tumors (**Supplemental Fig. 3A).** While IFNγ-producing T cells were seen in

442   CMT^{WT} tumors, a significantly greater density of IFNγ-producing CD4$^+$ and CD8$^+$ T cells was

443   seen in CMT167^{AhR-KO} tumors (**Supplemental Fig. 3B).**

444   Corresponding to this increase in total CD4$^+$ and CD8$^+$ T cells, the density of CD4$^+$PD-1$^+$

445   or CD8$^+$PD-1$^+$ T cells increased over time in the CMT167^{AhR-KO} but not in control tumors (**Fig.**

446   **7D**). Although associated with T cell exhaustion, high PD-1 levels on T cells have also been

447   positively associated with LUAD survival after anti-PD-1 therapy (74). In addition, PD-1 has

448   recently been shown to mark a subset of tumor neoantigen-specific tissue-resident memory T

449   cells in LUAD (74), HNSCC (75), colorectal cancer (75) and sarcoma (76). In this vein, the

450   density of CD4$^+$ or CD8$^+$ T cells expressing a CD44^{high} activated/memory phenotype increased

451   over time in the CMT167^{AhR-KO} but not in control tumors (**Fig. 7E**). Furthermore, the

452   percentages of CD4$^+$PD-1$^+$ or CD8$^+$PD-1$^+$ cells that were also CD44^{high} were significantly higher

453   in CMT167^{AhR-KO} tumors (**Fig. 7F**). These data suggest that tumor-infiltrating T cells in the

454   CMT167^{AhR-KO} tumors express more of an activation/memory phenotype than those from

455   wildtype tumors.

456   Finally, we note that 77% of the CMT167^{AhR-KO} cell-transplanted mice never grew

457   tumors and therefore were not evaluable for T cell infiltration. Therefore, analysis of only the

458   23% of CMT167^{AhR-KO} tumors that did form may underestimate the extent of T cell recruitment

459   during complete rejection of AhR-KO tumors.

460

461   **Single cell RNA-sequencing analysis of tumor-infiltrating T cells.**

462   To more definitively categorize tumor infiltrating T cell subsets, scRNA-seq was

463   performed on sorted CD45$^+$ immune cells (>90% viable) from digested 5-week tumors. SingleR

464   (42) and the ImmGen compendium (43) were used to identify T cell subtypes and the Seurat R

465   package (44) was used for clustering and differential gene expression (DGE) analysis. Clustering

466   of CD3 T cells resulted in 16 unique T cell clusters (#0-15) visualized in UMAP plots (**Fig. 8A**).

467   Five clusters were categorized as CD4 T cells (**Fig. 8B green dots; Fig. 8C left**) and 11 were

468   categorized as CD8 T cells (**Fig. 8B purple dots; Fig. 8D right**).

469   Quantifying the percentage of CD4 and CD8 T cells from CMT167^{WT} or CMT167^{AhR-KO}

470   tumors that are represented in each of the 16 CD3 clusters revealed that cluster 5 (CD4) and

471   clusters 2, 6 and 8 (CD8) consisted predominantly ($\geq$90%) of T cell subsets from CMT167^{WT}

472   tumors (**Fig. 8E burnt orange polygon, Fig. 8F**) whereas CD8 clusters 13 and 14 consisted

473   predominantly ($\geq$94%) of T cells from CMT167^{AhR-KO} tumors (**Fig. 8E teal polygon, Fig 8F**).

474   Notably, cluster 6 was unique to CD8 T cells from CMT167^{WT} tumors while cluster 13, which

475   expressed the highest level of *CD8a* (**Fig. 8D)**, was unique to T cells from CMT167^{AhR-KO}

476   tumors (**Fig. 8F**).

477   Gene set variation analysis (GSVA), a rank-based gene-set enrichment method used to

478   assess relative T cell activity [111], indicated that CD4 and CD8 T cells from CMT167^{AhR-KO}

479   tumors were significantly ($p<10^{-15}$ and $p<10^{-11}$ respectively) more active than those from

480   CMT167^{WT} tumors (**Fig 9A**). Pooling differentially expressed genes in CD8 clusters that were

481   comprised of >94% T cells from either CMT167^{WT} or CMT167^{AhR-KO} tumors demonstrated that

482   the aggregate of CD8 clusters 13+14 from CMT167^{AhR-KO} tumors was significantly more active

483   than the aggregate of CD8 clusters 2+6+8 from CMT167^{WT} tumors (**Fig. 9B, left**). The

484   difference in relative activity was even greater when comparing only the clusters that were 100%

485   unique to AhR-KO and wildtype tumors, i.e., cluster 6 (CMT167^{WT}) *vs* cluster 13 (CMT167^{AhR-}

486   ^{KO})(**Fig. 9B, right**).

487   One type of cell-cell communication that could account for the greater activity seen in

488   CD8 T cell clusters from CMT167^{AhR-KO} tumors would involve interactions of T cells with

489   antigen presenting cells (APC). Therefore, the CellChat cell-cell communication platform (45)

490   was used to estimate the number and strength (weight of cell interactions based on ligand-

491   receptor binding strength/probability) of incoming signaling from dendritic cells (DC),

22

492   macrophages (MΦ), and B cells to CD8 clusters, with a focus on clusters that represent >90% of

493   T cells from CMT167[WT] or CMT167[AhR-KO] tumors. CellChat estimated significantly more

494   incoming interactions (counts) from all three types of APC to the CMT167[AhR-KO] CD8 clusters

495   13+14 than from APC to the CMT167[WT] CD8 clusters 2+6+8 (**Fig. 9C, top left, red lines**). (The

496   color of the lines represents the tumor source of T cells and the thickness represents the relative

497   number of incoming signals from APC). The number of T-T cell interactions in clusters 13+14

498   was also greater than T cell interactions in clusters 2+6+8 (**Fig. 9C, black arrows**). Similarly,

499   the strength of incoming signals from DC or B cells and between T cells was greater for clusters

500   13+14 than for clusters 2+6+8 (**Fig. 9C, top right, red lines**). Relatively weak interactions

501   between MΦ and CMT167[WT] clusters 2+6+8 were noted (**Fig. 9C, top right, blue line**). When

502   comparing cluster 6 and 13, 100% CMT167[AhR-KO]-derived cluster 13 had significantly more and

503   stronger interactions with all three APC than 100% CMT167[WT]-derived cluster 6 (**Fig. 9C,**

504   **bottom)**.

505   To assess patterns of single gene expression that could point to cell function, particularly

506   for cluster 13, one (cluster)-vs-all differential analyses were performed considering only CD4 or

507   CD8 clusters with ≥90% representation from either wildtype or AhR-KO tumors. In particular

508   we assessed the relative expression of genes associated with T cell exhaustion/activation and

509   CD8^{+} T cell killing activity. CD4 cluster 5, 90% of which consisted of T cells from CMT167[WT]

510   tumors, expressed relatively high levels of *Tnfrs9* (CD137)(**Fig. 9D**), a marker which predicts

511   poorer survival in LUAD (77). Cluster 5 also expressed relatively high levels of *Tigit, Tgfß,*

512   *Pdcd1 (Pd-1))*, and *Ctla4*, a phenotype consistent with immunosuppressive or exhausted T cells

513   (78). Among the CD8 clusters (**Fig. 9E**), cluster 6, which is entirely composed of cells from

514   wildtype tumors, was the only CD8 cluster that expressed elevated levels of *Itgav, Tnfsrf9, Tigit,*

515   *Pdcd-1*, *Lag3*, and *Tim3* (*Havcr2*), all of which are associated with exhausted or

516   immunosuppressive CD8^{+} T cells (78-80). Conversely, the two clusters expressing the highest

517   levels of granzyme B (*Gzmb*), clusters 3 and 13, were composed of T cells predominantly

518   (cluster 3, 83%) or entirely (cluster 13, 100%) from AhR-KO tumors. Notably, cluster 13 was

519   the only cluster to express relatively high levels of <u>both</u> granzyme B and perforin (*Prf1*),

520   essential CTL effector molecules. In contrast, *Gzmb* and *Prf1* expression was either not

521   significantly different or significantly lower, relative to all other clusters, in three CD8 clusters

522   predominantly made up of T cells from wildtype tumors, i.e., clusters 2, 6 and 8.

523   Given that AhR-KO cluster 13 is apparently more active in general and more interactive

524   with APC than T cells from CMT167[WT] tumors, and that cluster 13 cells express higher *Gzmb*

525   and *Prf1* levels than the aggregate of all the other CD8 clusters, we postulated that it would

526   express a more robust global transcriptomic profile of an active CTL than other CD8 clusters.

527   Gene Set Enrichment Analysis (GSEA) was performed using the clusterProfiler package to test

528   this hypothesis. Three sets of upregulated genes in cluster 13 were generated relative to: 1) all

529   other CD8 clusters, 2) the aggregate of clusters 2, 6, and 8, and 3) cluster 6. Parameters were set

530   to a minimum of 25% expressing cells and a minimum average log2 fold change of 0.25. The

531   FindMarkers function with the MAST wrapper in Seurat was used to rank these DEG sets by

532   decreasing average log2 fold change (avg -log2FC) and adjusted p-value (-log10). The ranked

533   genes were then input into the GSEA enrichment function using the ImmunesigDB gene sets

534   from the MSigDB website. All three sets of genes upregulated in cluster 13 were significantly

535   enriched in six sets of genes experimentally shown to be upregulated in activated CD8 T cells

536   (**Fig. 9F**). These include three sets of genes upregulated in effector CD8 T cells as compared

537   with naïve CD8 T cells (GSE9650 Eff. vs Naïve CD8 T cells, Goldrath Eff. *vs* Naïve CD8 T

538   cells, Kaech Eff. *vs* Naïve CD8 T cells)(81, 82), two sets of genes upregulated in effector CD8 T

539   cells relative to memory CD8 T cells (GSE9650 Eff. *vs* Mem. CD8 T cells, Kaech Eff. *vs* Mem.

540   CD8 T cells)(81, 83) and one set of genes upregulated in activated CD8 T cells as compared with

541   tolerized CD8 T cells (GSE14699 Activated *vs* Tolerant CD8 T)(84)(**Fig. 9F**). All of these

542   results are consistent with the hypothesis that at least some subsets of CD8 T cells from

543   CMT167^{AhR-KO} tumors, including and especially cluster 13, are more active in the tumor

544   microenvironment than CD8 T cells from CMT167^{WT} tumors.

545   **Discussion**

546   The current studies were motivated in part by our incomplete understanding of factors

547   regulating immune checkpoints, the sometimes contradictory effects of IFNγ on tumor immunity,

548   and the accumulating data indicating an important role for the AhR in immune regulation in the

549   presence or absence of environmental agonists. Recent calls for AhR inhibitors as cancer

550   therapeutics (35, 85-88) and the initiation of cancer clinical trials with AhR inhibitors (89)

551   further add significance to the studies.

552   Our initial studies of global transcriptomic changes in murine and human LUAD cells

553   pointed to several pathways through which the AhR could control intrinsic drivers of cancer cells

554   as well as regulators of immune cells in the tumor microenvironment (TME). With regard to the

555   former, RNA-seq analysis of AhR-regulated genes revealed the potential for the AhR to control

556   expression of multiple genes implicated in LUAD. For example, *Egfr* expression was reduced

557   13-16 fold in murine and human LUAD cells, respectively, following AhR knockout (**Fig. 1**).

558   Elevated EGFR activity is a prognostic indicator in LUAD (52) and the EGFR itself is an

559   important therapeutic target (90, 91). Thrombospondin 1 (*Thbs1*), downregulated >45 fold in

560   both CMT167 and A549 cells after AhR knockout, is also a prognostic marker of LUAD

561   outcomes (51, 92). *Colra1*, downregulated 9-219 fold after AhR knockout, can regulate LUAD

562   metastasis (50).

563   With regard to malignant cell effects on the immune TME, bulk RNA-seq data

564   documented significant downregulation of the immune-related genes *Cccl2*, *Ccl5*, *ITGβ2*, *IDO1*,

565   and *CD274/PD-L1* following AhR deletion. The decrease in *Ccl2* after AhR deletion is

566   reminiscent of AhR control of the CCL2 receptor, CCR2, in glioblastoma (93) and with AhR

567   control of CCL2 expression in multiple organs after exposure to the prototypic AhR agonist

568   2,3,7,8-tetrachlorodibenzo(p)dioxin (TCDD) (94), in non-transformed endothelial cells (95), and

569   in triple negative breast cancer cells (96). AhR-driven expression of two chemokine genes, *Ccl2*

570   and *Ccl5*, could increase recruitment of immunosuppressive monocytes, dendritic cells, and T

571   cell subsets to the TME (97-99). Malignant cell ITGβ2 is associated with suppressive or

572   exhausted T cell infiltration in LUAD (53).

573   RT-qPCR studies confirmed the bulk RNA-seq data by demonstrating that baseline

574   *Cd274* and *Ido1/2* decreased in AhR-knockout CMT167 cells (**Figs. 3-5**). Conversely, treatment

575   of CMT167 cells with the environmental chemical and AhR agonist B(a)P increased *Cd274* and

576   *Ido1/2* expression (**Fig. 3**). These data expand on previous studies showing that cigarette smoke

577   increases PD-L1 on normal human epithelial cells (35) and help reveal a new mechanism for the

578   well-established immunosuppression generated in animal models by B(a)P and other

579   environmental AhR agonists. Furthermore, the ability of the AhR to regulate baseline levels of

580   PD-L1 and IDO is an important finding with clinical implications. For example, tumors with

581   relatively high AhR levels would be expected to be relatively dependent on the PD-1/PD-L1 axis

582   for immune escape. Indeed, tumors from ~81% of NSCLC patients who achieve a partial or

583   stable response to Pembrolizumab express relatively high AhR levels whereas tumors from

584   ~75% of patients that responded poorly or not at all to Pembrolizumab exhibit relatively low

585   AhR levels (35).

586   　　　Of particular interest were the results with IFNγ that highlighted the likelihood that this

587   cytokine, usually associated with T cell activation and tumor immunity, can also play a negative

588   immunoregulatory role in cancer in general (100, 101) and lung cancer in specific (102). That the

589   effects of IFNγ are mediated at least in part by the AhR is a central and novel finding of these

590   studies. LUAD cells are likely to be exposed to IFNγ *in situ* through infiltrating T cells, NK

591   cells, and/or neutrophils (**Fig. 10**).

592   　　　It is well established that IFNγ upregulates CD274/PD-L1 and IDO through the

593   JAK/STAT pathway (12, 69). Here we demonstrate that optimal expression of JAK/STAT

594   components (JAK2, STAT1, and STAT3) and critical immune checkpoints targeted by

595   JAK/STAT signaling, PD-L1, and IDO, is AhR dependent. These results suggest a novel

596   signaling pathway initiated or exacerbated by environmental or endogenous AhR ligands and

597   leading to suppression of tumor immunity (**Fig. 10**). If confirmed in other cell contexts, the data

598   would also suggest that the AhR may influence a variety of other important JAK/STAT-

599   dependent outcomes not evaluated here.

600   　　　The data presented here demonstrate that the AhR participates in an amplification loop in

601   LUAD cells by up-regulating IDO1 and IDO2, proximal enzymes in the Kyn pathway of

602   tryptophan metabolism, and resulting in production of endogenous AhR ligands including but

603   probably not limited to Kyn itself (**Fig. 10**). These AhR ligands not only continue to drive AhR

604   activity withing the malignant LUAD cells but may also contribute to immunosuppression in the

605   tumor microenvironment by inducing or recruiting AhR[+] Treg (103-105), tolerogenic dendritic

27

606   cells (24, 106), immunosuppressive macrophages (93), or myeloid-derived suppressor cells

607   (107). Thus, in this context, IFNγ can be viewed as a LUAD enabler through AhR regulation.

608   The finding that IFNγ induced *Cyp1a1* or *Cyp1b1* in CMT167 cells (**Figs. 4,5**) is

609   predicted to reflect IFNγ induction of IDO and the subsequent increase in Kyn (**Figs. 4,5**) or

610   other downstream tryptophan derived AhR ligands. That a cytokine so critical to immunity can

611   induce these canonical AhR-driven genes as well as IDO suggests a novel route to increased

612   CYP1A1 or CYP1B1 metabolic activity in any cell type within an IFNγ-producing leukocyte-

613   infiltrated TME.

614   One question that remains to be answered is how IFNγ influences AhR activity upstream

615   of AhR-induced IDO up-regulation (**Fig. 10**). There are several, mostly untested possibilities: 1)

616   IFNγ might increase AhR expression levels. However, in our hands, AhR mRNA and protein

617   levels did not increase with addition of IFNγ in either CMT167 or A549 cells (not shown). 2)

618   IFNγ may modify expression or function of AhR-associated proteins including HSP90, p23, Src,

619   AhR interacting protein (AIP), ARNT, or the AhR repressor (AhRR). To our knowledge there is

620   little to no evidence of IFNγ control of p23, Src, AIP, ARNT, or AhRR. Furthermore, in

621   preliminary experiments with IFNγ-stimulated A549 cells we saw no effect of IFNγ on *HSP90*,

622   *p23*, *SRC*, *AIP*, *ARNT*, or *AhRR* mRNAs by RNA-seq. That said, in one report, HSP90 inhibitors

623   blocked IFNγ-induced upregulation of immune checkpoints IDO1 and PD-L1 in pancreatic

624   ductal adenocarcinoma cells (108). 3) IFNγ may affect AhR activity through epigenetic

625   modeling of AhR target genes (109) lowering the threshold to AhR transcriptional activity. 4) In

626   our hands AhR knockout generally does not completely ablate IDO expression (e.g., **Figs. 3,4,5**).

627   Therefore, there may be some AhR- and or JAK/STAT-independent component to IFNγ

628   upregulation of IDO which would be expected to produce AhR ligands that prime the

629   AhR→IDO→AhR ligand amplification loop and result in the outcomes studied herein. To that

630   point, STAT1-independent IFNγ signaling has been documented (110). 5) Perhaps the most

631   likely pathway to IFNγ-mediated AhR up-regulation is through NF-κB. IFNγ induces NF-κB

632   signaling (111), components of which can bind to and modify AhR activity (112, 113). Clearly,

633   more experimentation is required to resolve how IFNγ affects AhR signaling.

634   Given the *in vitro* effects of AhR knockout, it was hypothesized that CMT167^{AhR-KO} cells

635   would either grow more slowly or not all by virtue of an enabled immune system. Indeed, only

636   23% of the mice grew CMT167^{AhR-KO} tumors (**Fig. 6A**) and those CMT167^{AhR-KO} tumors that did

637   grow grew at a significantly slower pace than control CMT167^{Cas9} or CMT167^{WT} tumors (e.g.,

638   **Fig. 6B**). Furthermore, mice re-challenged with CMT167^{WT} cells seven weeks after inoculation

639   with CMT167^{AhR-KO} cells exhibited significant resistance to outgrowth of wildtype tumors (**Fig.**

640   **6C,D**) demonstrating some level of immune memory. Again, these results speak to the

641   significance of AhR activity in malignant cells and the effects that this activity has on the

642   immune microenvironment. That some CMT167^{AhR-KO} tumors did escape immune attack

643   suggests that this model could prove useful in cataloguing mechanisms through which LUADs

644   being targeted with immune checkpoint inhibitors escape an otherwise competent immune

645   system. Experiments assessing the mechanism of immune escape are now underway.

646   Immunofluorescent studies gave the first hint that immune protection against

647   CMT167^{AhR-KO} tumors is likely mediated by CD45^{+} cells. Thus, while nearly absent in

648   CMT167^{WT} tumors, CD45^{+} TILs were plentiful in CMT167^{AhR-KO} tumors (**Fig. 7A**).

649   Immunophenotyping studies confirmed an abundance of CD4^{+} and CD8^{+} T cells in CMT167^{AhR-}

650   ^{KO} tumors (**Fig. 7C-E**). Although a significant percentage of these cells expressed PD-1, their

651   continued accumulation in CMT167^{AhR-KO} tumors over time and the single cell characterization

652   of interactive CD8 T cells suggests that they were not exhausted. Rather, they may represent a

653   population of PD1^{+} tumor antigen-specific CTL as seen in LUAD, colorectal cancer, and

654   HNSCC (74, 75).

655   More granular analysis of the T cell subsets by scRNA-sequencing revealed the presence

656   of 16 clusters of CD3 T cells, a demonstration of the molecular heterogeneity of tumor-

657   infiltrating T cells. Importantly, the distribution of these T cell subsets was significantly different

658   in CMT167[WT] vs CMT167[AhR-KO] tumors with one CD8 subset unique to wildtype tumors (cluster

659   6) and another unique to CMT167[AhR-KO] tumors (cluster 13). The only cluster that expressed

660   multiple markers of Tregs or exhausted T cells (*Tnfrs9*, *Tgfβ*, *Tigit*, *Pdcd1/Pd-1*, *Ctla4*) was a

661   CD4 cluster composed of predominantly (90%) T cells from wildtype tumors (cluster 5).

662   Similarly, CD8 cluster 6, composed 100% of T cells from wildtype tumors, expressed six

663   markers of exhausted T cells (*Itgav*, *Tnfsrf9*, *Tigit*, *Pdcd-1*, *Lag3*, and *Havcrw/Tim3*). In contrast,

664   CD8 cluster 13, composed 100% of T cells from AhR-KO tumors, expressed the highest levels

665   of granzyme B and perforin mRNAs. GSVA analysis indicated that this cluster was more active

666   than CD8 T cells from wildtype tumors and CellChat analyses supported the hypothesis that

667   these cells are actively engaged with APCs in the CMT167[AhR-KO] microenvironment. Indeed, it is

668   possible that the PD1 expressing cluster 13 cells represents activated tumor-specific CTL (114-

669   116). The only other CD8 subset to express high *Grzb* levels was also predominantly (83%)

670   made up of T cells from CMT167[AhR-KO] tumors. While additional functional studies would be

671   required to confirm the implied function of these clusters, the data are consistent with the

672   induction of an immunosuppressive TME by CMT[WT/Cas9] control cells and a more

673   immunocompetent TME in CMT167[AhR-KO] tumors. We note that these studies do not exclude a

674   role for non-T cells in LUAD AhR-mediated immunosuppression. Analysis of other TIL subsets

675   that are differentially represented in CMT167$^{\text{WT/Cas9}}$ and CMT167$^{\text{AhR-KO}}$ tumors, including

676   neutrophils, macrophages, dendritic cells, and B cells, is ongoing.

677　**Acknowledgements**

679

680　**References**

681　1.　Ferlay, J., H. R. Shin, F. Bray, D. Forman, C. Mathers, and D. M. Parkin. 2010. Estimates

682　　　of worldwide burden of cancer in 2008: GLOBOCAN 2008. *Int J Cancer* 127: 2893-

683　　　2917.

684　2.　Sainz de Aja, J., A. F. M. Dost, and C. F. Kim. 2021. Alveolar progenitor cells and the

685　　　origin of lung cancer. *J Intern Med* 289: 629-635.

686　3.　Rivera, G. A., and H. Wakelee. 2016. Lung Cancer in Never Smokers. *Adv Exp Med Biol*

687　　　893: 43-57.

688　4.　Sezer, A., S. Kilickap, M. Gumus, I. Bondarenko, M. Ozguroglu, M. Gogishvili, H. M.

689　　　Turk, I. Cicin, D. Bentsion, O. Gladkov, P. Clingan, V. Sriuranpong, N. Rizvi, B. Gao, S.

690　　　Li, S. Lee, K. McGuire, C. I. Chen, T. Makharadze, S. Paydas, M. Nechaeva, F. Seebach,

691　　　D. M. Weinreich, G. D. Yancopoulos, G. Gullo, I. Lowy, and P. Rietschel. 2021.

692　　　Cemiplimab monotherapy for first-line treatment of advanced non-small-cell lung cancer

693　　　with PD-L1 of at least 50%: a multicentre, open-label, global, phase 3, randomised,

694　　　controlled trial. *Lancet* 397: 592-604.

695　5.　Paz-Ares, L. G., S. S. Ramalingam, T. E. Ciuleanu, J. S. Lee, L. Urban, R. B. Caro, K.

696　　　Park, H. Sakai, Y. Ohe, M. Nishio, C. Audigier-Valette, J. A. Burgers, A. Pluzanski, R.

697　　　Sangha, C. Gallardo, M. Takeda, H. Linardou, L. Lupinacci, K. H. Lee, C. Caserta, M.

698　　　Provencio, E. Carcereny, G. A. Otterson, M. Schenker, B. Zurawski, A. Alexandru, A.

699　　　Vergnenegre, J. Raimbourg, K. Feeney, S. W. Kim, H. Borghaei, K. J. O'Byrne, M. D.

Hellmann, A. Memaj, F. E. Nathan, J. Bushong, P. Tran, J. R. Brahmer, and M. Reck.

2022. First-Line Nivolumab Plus Ipilimumab in Advanced NSCLC: 4-Year Outcomes

From the Randomized, Open-Label, Phase 3 CheckMate 227 Part 1 Trial. *J Thorac Oncol*

17: 289-308.

6. Opitz, C. A., U. M. Litzenburger, F. Sahm, M. Ott, I. Tritschler, S. Trump, T.

Schumacher, L. Jestaedt, D. Schrenk, M. Weller, M. Jugold, G. J. Guillemin, C. L.

Miller, C. Lutz, B. Radlwimmer, I. Lehmann, A. von Deimling, W. Wick, and M. Platten.

2011. An endogenous tumour-promoting ligand of the human aryl hydrocarbon receptor.

Nature 478: 197-203.

7. Liu, Y., X. Liang, W. Dong, Y. Fang, J. Lv, T. Zhang, R. Fiskesund, J. Xie, J. Liu, X.

Yin, X. Jin, D. Chen, K. Tang, J. Ma, H. Zhang, J. Yu, J. Yan, H. Liang, S. Mo, F.

Cheng, Y. Zhou, H. Zhang, J. Wang, J. Li, Y. Chen, B. Cui, Z. W. Hu, X. Cao, F. Xiao-

Feng Qin, and B. Huang. 2018. Tumor-repopulating cells induce PD-1 expression in

CD8(+) T cells by transferring kynurenine and AhR activation. *Cancer Cell* 33: 480-494

e487.

8. Amobi-McCloud, A., R. Muthuswamy, S. Battaglia, H. Yu, T. Liu, J. Wang, V. Putluri,

P. K. Singh, F. Qian, R. Y. Huang, N. Putluri, T. Tsuji, A. A. Lugade, S. Liu, and K.

Odunsi. 2021. IDO1 Expression in Ovarian Cancer Induces PD-1 in T Cells via Aryl

Hydrocarbon Receptor Activation. *Front Immunol* 12: 678999.

9. Litzenburger, U. M., C. A. Opitz, F. Sahm, K. J. Rauschenbach, S. Trump, M. Winter, M.

Ott, K. Ochs, C. Lutz, X. Liu, N. Anastasov, I. Lehmann, T. Hofer, A. von Deimling, W.

Wick, and M. Platten. 2014. Constitutive IDO expression in human cancer is sustained by

33

722   an autocrine signaling loop involving IL-6, STAT3 and the AHR. *Oncotarget* 5: 1038-

723   1051.

724 10. Mishra, A. K., T. Kadoishi, X. Wang, E. Driver, Z. Chen, X. J. Wang, and J. H. Wang.

725   2016. Squamous cell carcinomas escape immune surveillance via inducing chronic

726   activation and exhaustion of CD8+ T Cells co-expressing PD-1 and LAG-3 inhibitory

727   receptors. *Oncotarget* 7: 81341-81356.

728 11. Zhang, X., X. Liu, W. Zhou, Q. Du, M. Yang, Y. Ding, and R. Hu. 2021. Blockade of

729   IDO-Kynurenine-AhR Axis Ameliorated Colitis-Associated Colon Cancer via Inhibiting

730   Immune Tolerance. *Cell Mol Gastroenterol Hepatol* 12: 1179-1199.

731 12. Mandai, M., J. Hamanishi, K. Abiko, N. Matsumura, T. Baba, and I. Konishi. 2016. Dual

732   Faces of IFNgamma in Cancer Progression: A Role of PD-L1 Induction in the

733   Determination of Pro- and Antitumor Immunity. *Clin Cancer Res* 22: 2329-2334.

734 13. Mimura, K., J. L. Teh, H. Okayama, K. Shiraishi, L. F. Kua, V. Koh, D. T. Smoot, H.

735   Ashktorab, T. Oike, Y. Suzuki, Z. Fazreen, B. R. Asuncion, A. Shabbir, W. P. Yong, J.

736   So, R. Soong, and K. Kono. 2018. PD-L1 expression is mainly regulated by interferon

737   gamma associated with JAK-STAT pathway in gastric cancer. *Cancer Sci* 109: 43-53.

738 14. Gu, Y. Z., J. B. Hogenesch, and C. A. Bradfield. 2000. The PAS superfamily: sensors of

739   environmental and developmental signals. *Annu Rev Pharmacol Toxicol* 40: 519-561.

740 15. Holme, J. A., J. Vondracek, M. Machala, D. Lagadic-Gossmann, C. F. A. Vogel, E. Le

741   Ferrec, L. Sparfel, and J. Ovrevik. 2023. Lung cancer associated with combustion

742   particles and fine particulate matter (PM(2.5)) - The roles of polycyclic aromatic

743   hydrocarbons (PAHs) and the aryl hydrocarbon receptor (AhR). *Biochem Pharmacol*

744   216: 115801.

16. Tsay, J. J., K. M. Tchou-Wong, A. K. Greenberg, H. Pass, and W. N. Rom. 2013. Aryl hydrocarbon receptor and lung cancer. *Anticancer Res* 33: 1247-1256.

17. Mandal, P. K. 2005. Dioxin: a review of its environmental effects and its aryl hydrocarbon receptor biology. *J Comp Physiol B* 175: 221-230.

18. Nebert, D. W., A. Puga, and V. Vasiliou. 1993. Role of the Ah receptor and the dioxin-inducible [Ah] gene battery in toxicity, cancer, and signal transduction. *Ann N Y Acad Sci* 685: 624-640.

19. Quintana, F. J. 2013. Regulation of central nervous system autoimmunity by the aryl hydrocarbon receptor. *Semin Immunopathol* 35: 627-635.

20. Bruhs, A., T. Haarmann-Stemmann, K. Frauenstein, J. Krutmann, T. Schwarz, and A. Schwarz. 2015. Activation of the arylhydrocarbon receptor causes immunosuppression primarily by modulating dendritic cells. *J Invest Dermatol* 135: 435-444.

21. Campesato, L. F., S. Budhu, J. Tchaicha, C. H. Weng, M. Gigoux, I. J. Cohen, D. Redmond, L. Mangarin, S. Pourpe, C. Liu, R. Zappasodi, D. Zamarin, J. Cavanaugh, A. C. Castro, M. G. Manfredi, K. McGovern, T. Merghoub, and J. D. Wolchok. 2020. Blockade of the AHR restricts a Treg-macrophage suppressive axis induced by L-Kynurenine. *Nat Commun* 11: 4011.

22. Mezrich, J. D., J. H. Fechner, X. Zhang, B. P. Johnson, W. J. Burlingham, and C. A. Bradfield. 2010. An interaction between kynurenine and the aryl hydrocarbon receptor can generate regulatory T cells. *J Immunol* 185: 3190-3198.

23. Quintana, F. J., and D. H. Sherr. 2013. Aryl hydrocarbon receptor control of adaptive immunity. *Pharmacological reviews* 65: 1148-1161.

35

767   24.   Nguyen, N. T., A. Kimura, T. Nakahama, I. Chinen, K. Masuda, K. Nohara, Y. Fujii-

768   Kuriyama, and T. Kishimoto. 2010. Aryl hydrocarbon receptor negatively regulates

769   dendritic cell immunogenicity via a kynurenine-dependent mechanism. *Proc Natl Acad*

770   *Sci U S A* 107: 19961-19966.

771   25.   Moyer, B. J., I. Y. Rojas, I. A. Murray, S. Lee, H. F. Hazlett, G. H. Perdew, and C. R.

772   Tomlinson. 2017. Indoleamine 2,3-dioxygenase 1 (IDO1) inhibitors activate the aryl

773   hydrocarbon receptor. *Toxicol Appl Pharmacol* 323: 74-80.

774   26.   Murray, I. A., A. D. Patterson, and G. H. Perdew. 2014. Aryl hydrocarbon receptor

775   ligands in cancer: friend and foe. *Nat Rev Cancer* 14: 801-814.

776   27.   Novikov, O., Z. Wang, E. A. Stanford, A. J. Parks, A. Ramirez-Cardenas, E. Landesman,

777   I. Laklouk, C. Sarita-Reyes, D. Gusenleitner, A. Li, S. Monti, S. Manteiga, K. Lee, and

778   D. H. Sherr. 2016. An aryl hydrocarbon receptor-mediated amplification loop that

779   enforces cell migration in ER-/PR-/Her2- human breast cancer cells. *Mol Pharmacol* 90:

780   674-688.

781   28.   Stanford, E. A., Z. Wang, O. Novikov, F. Mulas, E. Landesman-Bollag, S. Monti, B. W.

782   Smith, D. C. Seldin, G. J. Murphy, and D. H. Sherr. 2016. The role of the aryl

783   hydrocarbon receptor in the development of cells with the molecular and functional

784   characteristics of cancer stem-like cells. *BMC Biol* 14: 20.

785   29.   Prud'homme, G. J. 2012. Cancer stem cells and novel targets for antitumor strategies.

786   *Curr Pharm Des* 18: 2838-2849.

787   30.   Therachiyil, L., R. Krishnankutty, F. Ahmad, J. M. Mateo, S. Uddin, and H. M. Korashy.

788   2022. Aryl Hydrocarbon Receptor Promotes Cell Growth, Stemness Like Characteristics,

789   and Metastasis in Human Ovarian Cancer via Activation of PI3K/Akt, beta-Catenin, and

790   Epithelial to Mesenchymal Transition Pathways. *Int J Mol Sci* 23.

791 31.   Rejano-Gordillo, C., A. Ordiales-Talavero, A. Nacarino-Palma, J. M. Merino, F. J.

792   Gonzalez-Rico, and P. M. Fernandez-Salguero. 2022. Aryl Hydrocarbon Receptor: From

793   Homeostasis to Tumor Progression. *Front Cell Dev Biol* 10: 884004.

794 32.   Ye, M., Y. Zhang, H. Gao, Y. Xu, P. Jing, J. Wu, X. Zhang, J. Xiong, C. Dong, L. Yao, J.

795   Zhang, and J. Zhang. 2018. Activation of the Aryl Hydrocarbon Receptor Leads to

796   Resistance to EGFR TKIs in Non-Small Cell Lung Cancer by Activating Src-mediated

797   Bypass Signaling. *Clin Cancer Res* 24: 1227-1239.

798 33.   Vrzalova, A., P. Pecinkova, P. Illes, S. Gurska, P. Dzubak, M. Szotkowski, M. Hajduch,

799   S. Mani, and Z. Dvorak. 2022. Mixture Effects of Tryptophan Intestinal Microbial

800   Metabolites on Aryl Hydrocarbon Receptor Activity. *Int J Mol Sci* 23.

801 34.   Hubbard, T. D., I. A. Murray, W. H. Bisson, T. S. Lahoti, K. Gowda, S. G. Amin, A. D.

802   Patterson, and G. H. Perdew. 2015. Adaptation of the human aryl hydrocarbon receptor to

803   sense microbiota-derived indoles. *Sci Rep* 5: 12689.

804 35.   Wang, G. Z., L. Zhang, X. C. Zhao, S. H. Gao, L. W. Qu, H. Yu, W. F. Fang, Y. C. Zhou,

805   F. Liang, C. Zhang, Y. C. Huang, Z. Liu, Y. X. Fu, and G. B. Zhou. 2019. The aryl

806   hydrocarbon receptor mediates tobacco-induced PD-L1 expression and is associated with

807   response to immunotherapy. *Nat Commun* 10: 1125.

808 36.   Kenison, J. E., Z. Wang, K. Yang, M. Snyder, F. J. Quintana, and D. H. Sherr. 2021. The

809   aryl hydrocarbon receptor suppresses immunity to oral squamous cell carcinoma through

810   immune checkpoint regulation. *Proc Natl Acad Sci U S A* 118.

811 37. Li, H. Y., M. McSharry, B. Bullock, T. T. Nguyen, J. Kwak, J. M. Poczobutt, T. R.

812 Sippel, L. E. Heasley, M. C. Weiser-Evans, E. T. Clambey, and R. A. Nemenoff. 2017.

813 The Tumor Microenvironment Regulates Sensitivity of Murine Lung Tumors to PD-

814 1/PD-L1 Antibody Blockade. *Cancer Immunol Res* 5: 767-777.

815 38. Liao, H., X. Chang, L. Gao, C. Ye, Y. Qiao, L. Xie, J. Lin, S. Cai, and H. Dong. 2023.

816 IL-17A promotes tumorigenesis and upregulates PD-L1 expression in non-small cell lung

817 cancer. *J Transl Med* 21: 828.

818 39. Nawas, A. F., A. Solmonson, B. Gao, R. J. DeBerardinis, J. D. Minna, M. Conacci-

819 Sorrell, and C. R. Mendelson. 2023. IL-1beta mediates the induction of immune

820 checkpoint regulators IDO1 and PD-L1 in lung adenocarcinoma cells. *Cell Commun*

821 *Signal* 21: 331.

822 40. Sanjana, N. E., O. Shalem, and F. Zhang. 2014. Improved vectors and genome-wide

823 libraries for CRISPR screening. *Nat Methods* 11: 783-784.

824 41. Hong, R., Y. Koga, S. Bandyadka, A. Leshchyk, Y. Wang, V. Akavoor, X. Cao, I.

825 Sarfraz, Z. Wang, S. Alabdullatif, F. Jansen, M. Yajima, W. E. Johnson, and J. D.

826 Campbell. 2022. Comprehensive generation, visualization, and reporting of quality

827 control metrics for single-cell RNA sequencing data. *Nat Commun* 13: 1688.

828 42. Aran, D., A. P. Looney, L. Liu, E. Wu, V. Fong, A. Hsu, S. Chak, R. P. Naikawadi, P. J.

829 Wolters, A. R. Abate, A. J. Butte, and M. Bhattacharya. 2019. Reference-based analysis

830 of lung single-cell sequencing reveals a transitional profibrotic macrophage. *Nat Immunol*

831 20: 163-172.

832   43.   Heng, T. S., M. W. Painter, and C. Immunological Genome Project. 2008. The

833   Immunological Genome Project: networks of gene expression in immune cells. *Nat*

834   *Immunol* 9: 1091-1094.

835   44.   Stuart, T., A. Butler, P. Hoffman, C. Hafemeister, E. Papalexi, W. M. Mauck, 3rd, Y.

836   Hao, M. Stoeckius, P. Smibert, and R. Satija. 2019. Comprehensive Integration of Single-

837   Cell Data. *Cell* 177: 1888-1902 e1821.

838   45.   Jin, S., C. F. Guerrero-Juarez, L. Zhang, I. Chang, R. Ramos, C. H. Kuan, P. Myung, M.

839   V. Plikus, and Q. Nie. 2021. Inference and analysis of cell-cell communication using

840   CellChat. *Nat Commun* 12: 1088.

841   46.   Hanzelmann, S., R. Castelo, and J. Guinney. 2013. GSVA: gene set variation analysis for

842   microarray and RNA-seq data. *BMC Bioinformatics* 14: 7.

843   47.   Newman, A. M., C. B. Steen, C. L. Liu, A. J. Gentles, A. A. Chaudhuri, F. Scherer, M. S.

844   Khodadoust, M. S. Esfahani, B. A. Luca, D. Steiner, M. Diehn, and A. A. Alizadeh.

845   2019. Determining cell type abundance and expression from bulk tissues with digital

846   cytometry. *Nat Biotechnol* 37: 773-782.

847   48.   Finak, G., A. McDavid, M. Yajima, J. Deng, V. Gersuk, A. K. Shalek, C. K. Slichter, H.

848   W. Miller, M. J. McElrath, M. Prlic, P. S. Linsley, and R. Gottardo. 2015. MAST: a

849   flexible statistical framework for assessing transcriptional changes and characterizing

850   heterogeneity in single-cell RNA sequencing data. *Genome Biol* 16: 278.

851   49.   Huang, X., Q. Sun, C. Chen, Y. Zhang, X. Kang, J. Y. Zhang, D. W. Ma, L. Xia, L. Xu,

852   X. Y. Xu, and B. H. Ren. 2017. MUC1 overexpression predicts worse survival in patients

853   with non-small cell lung cancer: evidence from an updated meta-analysis. *Oncotarget* 8:

854   90315-90326.

855   50.   Liu, W., H. Wei, Z. Gao, G. Chen, Y. Liu, X. Gao, G. Bai, S. He, T. Liu, W. Xu, X.

856   Yang, J. Jiao, and J. Xiao. 2018. COL5A1 may contribute the metastasis of lung

857   adenocarcinoma. *Gene* 665: 57-66.

858   51.   Sun, R., X. Meng, W. Wang, B. Liu, X. Lv, J. Yuan, L. Zeng, Y. Chen, B. Yuan, and S.

859   Yang. 2019. Five genes may predict metastasis in non-small cell lung cancer using

860   bioinformatics analysis. *Oncol Lett* 18: 1723-1732.

861   52.   Gao, M. G., S. Z. Wang, K. H. Han, S. N. Xie, and Q. Y. Liu. 2022. Clinical

862   characteristics and prognostic value of EGFR mutation in stage I lung adenocarcinoma

863   with spread through air spaces after surgical resection. *Neoplasma* 69: 1480-1489.

864   53.   Wu, J., W. Wang, Z. Li, and X. Ye. 2022. The prognostic and immune infiltration role of

865   ITGB superfamily members in non-small cell lung cancer. *Am J Transl Res* 14: 6445-

866   6466.

867   54.   Zu, L., J. He, N. Zhou, J. Zeng, Y. Zhu, Q. Tang, X. Jin, L. Zhang, and S. Xu. 2022. The

868   Profile and Clinical Significance of ITGB2 Expression in Non-Small-Cell Lung Cancer. *J

869   Clin Med* 11.

870   55.   Lee, K. Y., P. W. Shueng, C. M. Chou, B. X. Lin, M. H. Lin, D. Y. Kuo, I. L. Tsai, S. M.

871   Wu, and C. W. Lin. 2020. Elevation of CD109 promotes metastasis and drug resistance

872   in lung cancer via activation of EGFR-AKT-mTOR signaling. *Cancer Sci* 111: 1652-

873   1662.

874   56.   Fridlender, Z. G., V. Kapoor, G. Buchlis, G. Cheng, J. Sun, L. C. Wang, S. Singhal, L. A.

875   Snyder, and S. M. Albelda. 2011. Monocyte chemoattractant protein-1 blockade inhibits

876   lung cancer tumor growth by altering macrophage phenotype and activating CD8+ cells.

877   *Am J Respir Cell Mol Biol* 44: 230-237.

bioRxiv preprint doi: https://doi.org/10.1101/2024.08.12.607602; this version posted August 13, 2024. The copyright holder for this preprint (which was not certified by peer review) is the author/funder, who has granted bioRxiv a license to display the preprint in perpetuity. It is made available under aCC-BY-NC-ND 4.0 International license.

57. Melese, E. S., E. Franks, R. A. Cederberg, B. T. Harbourne, R. Shi, B. J. Wadsworth, J. L. Collier, E. C. Halvorsen, F. Johnson, J. Luu, M. H. Oh, V. Lam, G. Krystal, S. B. Hoover, M. Raffeld, R. M. Simpson, A. M. Unni, W. L. Lam, S. Lam, N. Abraham, K. L. Bennewith, and W. W. Lockwood. 2022. CCL5 production in lung cancer cells leads to an altered immune microenvironment and promotes tumor development. *Oncoimmunology* 11: 2010905.

58. Kocher, F., A. Amann, K. Zimmer, S. Geisler, D. Fuchs, R. Pichler, D. Wolf, K. Kurz, A. Seeber, and A. Pircher. 2021. High indoleamine-2,3-dioxygenase 1 (IDO) activity is linked to primary resistance to immunotherapy in non-small cell lung cancer (NSCLC). *Transl Lung Cancer Res* 10: 304-313.

59. Han, Y., Y. Zhang, Y. Tian, M. Zhang, C. Xiang, Q. Zhen, J. Liu, Y. Shang, Y. Zhao, H. Si, and A. Sui. 2022. The Interaction of the IFNgamma/JAK/STAT1 and JAK/STAT3 Signalling Pathways in EGFR-Mutated Lung Adenocarcinoma Cells. *J Oncol* 2022: 9016296.

60. Kado, S. Y., K. Bein, A. R. Castaneda, A. A. Pouraryan, N. Garrity, Y. Ishihara, A. Rossi, T. Haarmann-Stemmann, C. A. Sweeney, and C. F. A. Vogel. 2023. Regulation of IDO2 by the Aryl Hydrocarbon Receptor (AhR) in Breast Cancer. *Cells* 12.

61. Bekki, K., H. Vogel, W. Li, T. Ito, C. Sweeney, T. Haarmann-Stemmann, F. Matsumura, and C. F. Vogel. 2015. The aryl hydrocarbon receptor (AhR) mediates resistance to apoptosis induced in breast cancer cells. *Pestic Biochem Physiol* 120: 5-13.

62. Vogel, C. F., S. R. Goth, B. Dong, I. N. Pessah, and F. Matsumura. 2008. Aryl hydrocarbon receptor signaling mediates expression of indoleamine 2,3-dioxygenase. *Biochem Biophys Res Commun* 375: 331-335.

41

901   63.   Bankoti, J., B. Rase, T. Simones, and D. M. Shepherd. 2010. Functional and phenotypic

902   effects of AhR activation in inflammatory dendritic cells. *Toxicol Appl Pharmacol* 246:

903   18-28.

904   64.   Muller, A. J., M. G. Manfredi, Y. Zakharia, and G. C. Prendergast. 2019. Inhibiting IDO

905   pathways to treat cancer: lessons from the ECHO-301 trial and beyond. *Semin*

906   *Immunopathol* 41: 41-48.

907   65.   Fujiwara, Y., S. Kato, M. K. Nesline, J. M. Conroy, P. DePietro, S. Pabla, and R.

908   Kurzrock. 2022. Indoleamine 2,3-dioxygenase (IDO) inhibitors and cancer

909   immunotherapy. *Cancer Treat Rev* 110: 102461.

910   66.   Powderly, J. D., S. J. Klempner, A. Naing, J. Bendell, I. Garrido-Laguna, D. V. T.

911   Catenacci, M. H. Taylor, J. J. Lee, F. Zheng, F. Zhou, X. Gong, H. Gowda, and G. L.

912   Beatty. 2022. Epacadostat Plus Pembrolizumab and Chemotherapy for Advanced Solid

913   Tumors: Results from the Phase I/II ECHO-207/KEYNOTE-723 Study. *Oncologist* 27:

914   905-e848.

915   67.   Zhang, Y., Z. Hu, J. Zhang, C. Ren, and Y. Wang. 2022. Dual-target inhibitors of

916   indoleamine 2, 3 dioxygenase 1 (Ido1): A promising direction in cancer immunotherapy.

917   *Eur J Med Chem* 238: 114524.

918   68.   El Jamal, S. M., E. B. Taylor, Z. Y. Abd Elmageed, A. A. Alamodi, D. Selimovic, A.

919   Alkhateeb, M. Hannig, S. Y. Hassan, S. Santourlidis, P. L. Friedlander, Y. Haikel, S.

920   Vijaykumar, E. Kandil, and M. Hassan. 2016. Interferon gamma-induced apoptosis of

921   head and neck squamous cell carcinoma is connected to indoleamine-2,3-dioxygenase via

922   mitochondrial and ER stress-associated pathways. *Cell Div* 11: 11.

923 69. Zhu, J., Y. Li, and X. Lv. 2022. IL4I1 enhances PD-L1 expression through JAK/STAT

924   signaling pathway in lung adenocarcinoma. *Immunogenetics*.

925 70. Iwasaki, T., K. Kohashi, Y. Toda, S. Ishihara, Y. Yamada, and Y. Oda. 2021. Association

926   of PD-L1 and IDO1 expression with JAK-STAT pathway activation in soft-tissue

927   leiomyosarcoma. *J Cancer Res Clin Oncol* 147: 1451-1463.

928 71. Kazan, O., G. Kir, M. Culpan, G. E. Cecikoglu, G. Atis, and A. Yildirim. 2022. The

929   association between PI3K, JAK/STAT pathways with the PDL-1 expression in prostate

930   cancer. *Andrologia* 54: e14541.

931 72. Li, C., F. Yang, R. Wang, W. Li, N. Maskey, W. Zhang, Y. Guo, S. Liu, H. Wang, and X.

932   Yao. 2021. CALD1 promotes the expression of PD-L1 in bladder cancer via the

933   JAK/STAT signaling pathway. *Ann Transl Med* 9: 1441.

934 73. Horvath, C. M. 2004. The Jak-STAT pathway stimulated by interferon gamma. *Sci STKE*

935   2004: tr8.

936 74. Thommen, D. S., V. H. Koelzer, P. Herzig, A. Roller, M. Trefny, S. Dimeloe, A.

937   Kiialainen, J. Hanhart, C. Schill, C. Hess, S. Savic Prince, M. Wiese, D. Lardinois, P. C.

938   Ho, C. Klein, V. Karanikas, K. D. Mertz, T. N. Schumacher, and A. Zippelius. 2018. A

939   transcriptionally and functionally distinct PD-1(+) CD8(+) T cell pool with predictive

940   potential in non-small-cell lung cancer treated with PD-1 blockade. *Nat Med* 24: 994-

941   1004.

942 75. Duhen, R., O. Fesneau, K. A. Samson, A. K. Frye, M. Beymer, V. Rajamanickam, D.

943   Ross, E. Tran, B. Bernard, A. D. Weinberg, and T. Duhen. 2022. PD-1 and ICOS

944   coexpression identifies tumor-reactive CD4+ T cells in human solid tumors. *J Clin Invest*

945   132.

76. Alspach, E., D. M. Lussier, A. P. Miceli, I. Kizhvatov, M. DuPage, A. M. Luoma, W. Meng, C. F. Lichti, E. Esaulova, A. N. Vomund, D. Runci, J. P. Ward, M. M. Gubin, R. F. V. Medrano, C. D. Arthur, J. M. White, K. C. F. Sheehan, A. Chen, K. W. Wucherpfennig, T. Jacks, E. R. Unanue, M. N. Artyomov, and R. D. Schreiber. 2019. MHC-II neoantigens shape tumour immunity and response to immunotherapy. *Nature* 574: 696-701.

77. Cho, J. W., J. Son, S. J. Ha, and I. Lee. 2021. Systems biology analysis identifies TNFRSF9 as a functional marker of tumor-infiltrating regulatory T-cell enabling clinical outcome prediction in lung cancer. *Comput Struct Biotechnol J* 19: 860-868.

78. Miragaia, R. J., T. Gomes, A. Chomka, L. Jardine, A. Riedel, A. N. Hegazy, N. Whibley, A. Tucci, X. Chen, I. Lindeman, G. Emerton, T. Krausgruber, J. Shields, M. Haniffa, F. Powrie, and S. A. Teichmann. 2019. Single-Cell Transcriptomics of Regulatory T Cells Reveals Trajectories of Tissue Adaptation. *Immunity* 50: 493-504 e497.

79. Mair, I., S. E. J. Zandee, I. S. Toor, L. Saul, R. C. McPherson, M. D. Leech, D. J. Smyth, R. A. O'Connor, N. C. Henderson, and S. M. Anderton. 2018. A Context-Dependent Role for alphav Integrins in Regulatory T Cell Accumulation at Sites of Inflammation. *Front Immunol* 9: 264.

80. Edwards, J. P., A. M. Thornton, and E. M. Shevach. 2014. Release of active TGF-beta1 from the latent TGF-beta1/GARP complex on T regulatory cells is mediated by integrin beta8. *J Immunol* 193: 2843-2849.

81. Kaech, S. M., S. Hemby, E. Kersh, and R. Ahmed. 2002. Molecular and functional profiling of memory CD8 T cell differentiation. *Cell* 111: 837-851.

44

968   82.   Luckey, C. J., D. Bhattacharya, A. W. Goldrath, I. L. Weissman, C. Benoist, and D.

969   Mathis. 2006. Memory T and memory B cells share a transcriptional program of self-

970   renewal with long-term hematopoietic stem cells. *Proc Natl Acad Sci U S A* 103: 3304-

971   3309.

972   83.   Wherry, E. J., S. J. Ha, S. M. Kaech, W. N. Haining, S. Sarkar, V. Kalia, S.

973   Subramaniam, J. N. Blattman, D. L. Barber, and R. Ahmed. 2007. Molecular signature of

974   CD8+ T cell exhaustion during chronic viral infection. *Immunity* 27: 670-684.

975   84.   Parish, I. A., S. Rao, G. K. Smyth, T. Juelich, G. S. Denyer, G. M. Davey, A. Strasser,

976   and W. R. Heath. 2009. The molecular signature of CD8+ T cells undergoing deletional

977   tolerance. *Blood* 113: 4575-4585.

978   85.   Paris, A., N. Tardif, F. M. Baietti, C. Berra, H. M. Leclair, E. Leucci, M. D. Galibert, and

979   S. Corre. 2022. The AhR-SRC axis as a therapeutic vulnerability in BRAFi-resistant

980   melanoma. *EMBO Mol Med* 14: e15677.

981   86.   Morrow, D., C. Qin, R. Smith, 3rd, and S. Safe. 2004. Aryl hydrocarbon receptor-

982   mediated inhibition of LNCaP prostate cancer cell growth and hormone-induced

983   transactivation. *J Steroid Biochem Mol Biol* 88: 27-36.

984   87.   Martano, M., P. Stiuso, A. Facchiano, S. De Maria, D. Vanacore, B. Restucci, C. Rubini,

985   M. Caraglia, G. Ravagnan, and L. Lo Muzio. 2018. Aryl hydrocarbon receptor, a tumor

986   grade associated marker of oral cancer, is directly downregulated by polydatin: A pilot

987   study. *Oncol Rep* 40: 1435-1442.

988   88.   McGovern, K., A. C. Castro, J. Cavanaugh, S. Coma, M. Walsh, J. Tchaicha, S. Syed, P.

989   Natarajan, M. Manfredi, X. M. Zhang, and J. Ecsedy. 2022. Discovery and

990 Characterization of a Novel Aryl Hydrocarbon Receptor Inhibitor, IK-175, and Its

991 Inhibitory Activity on Tumor Immune Suppression. *Mol Cancer Ther* 21: 1261-1272.

992 89. McKean, M., D. Aggen, N. Lakhani, B. Bashir, J. Luke, J. Hoffman-Censits, D. Alhalabi,

993 I. Bowman, E. Guancial, A. Tan, T. Lingaraj, M. Timothy, K. Kacena, K. Malek, and S.

994 Santillana. 2022. Phase 1a/b open-label study of IK-175, an oral AHR inhibitor, alone

995 and in combination with nivolumab in patients with locally advanced or metastatic solid

996 tumors and urothelial carcinoma. *J. Clin. Onc.* 40.

997 90. Li, J., P. Chen, Q. Wu, L. Guo, K. W. Leong, K. I. Chan, and H. F. Kwok. 2022. A novel

998 combination treatment of antiADAM17 antibody and erlotinib to overcome acquired drug

999 resistance in non-small cell lung cancer through the FOXO3a/FOXM1 axis. *Cell Mol Life*

1000 *Sci* 79: 614.

1001 91. Lee, Y., H. R. Kim, M. H. Hong, K. H. Lee, K. U. Park, G. K. Lee, H. Y. Kim, S. H. Lee,

1002 K. Y. Lim, S. J. Yoon, B. C. Cho, and J. Y. Han. 2023. A randomized Phase 2 study to

1003 compare erlotinib with or without bevacizumab in previously untreated patients with

1004 advanced non-small cell lung cancer with EGFR mutation. *Cancer* 129: 405-414.

1005 92. Li, R., X. Liu, X. J. Zhou, X. Chen, J. P. Li, Y. H. Yin, and Y. Q. Qu. 2020. Identification

1006 and validation of the prognostic value of immune-related genes in non-small cell lung

1007 cancer. *Am J Transl Res* 12: 5844-5865.

1008 93. Takenaka, M. C., G. Gabriely, V. Rothhammer, I. D. Mascanfroni, M. A. Wheeler, C. C.

1009 Chao, C. Gutierrez-Vazquez, J. Kenison, E. C. Tjon, A. Barroso, T. Vandeventer, K. A.

1010 de Lima, S. Rothweiler, L. Mayo, S. Ghannam, S. Zandee, L. Healy, D. Sherr, M. F.

1011 Farez, A. Prat, J. Antel, D. A. Reardon, H. Zhang, S. C. Robson, G. Getz, H. L. Weiner,

46

1012   and F. J. Quintana. 2020. Control of tumor-associated macrophages and T cells in

1013   glioblastoma via AHR and CD39. *Nat Neurosci* 22: 729-740.

1014   94.   Vogel, C. F., N. Nishimura, E. Sciullo, P. Wong, W. Li, and F. Matsumura. 2007.

1015   Modulation of the chemokines KC and MCP-1 by 2,3,7,8-tetrachlorodibenzo-p-dioxin

1016   (TCDD) in mice. *Arch Biochem Biophys* 461: 169-175.

1017   95.   Watanabe, I., J. Tatebe, S. Namba, M. Koizumi, J. Yamazaki, and T. Morita. 2013.

1018   Activation of aryl hydrocarbon receptor mediates indoxyl sulfate-induced monocyte

1019   chemoattractant protein-1 expression in human umbilical vein endothelial cells. *Circ J*

1020   77: 224-230.

1021   96.   Goode, G., S. Pratap, and S. E. Eltom. 2014. Depletion of the aryl hydrocarbon receptor

1022   in MDA-MB-231 human breast cancer cells altered the expression of genes in key

1023   regulatory pathways of cancer. *PLoS One* 9: e100103.

1024   97.   Li, L., Y. D. Liu, Y. T. Zhan, Y. H. Zhu, Y. Li, D. Xie, and X. Y. Guan. 2018. High

1025   levels of CCL2 or CCL4 in the tumor microenvironment predict unfavorable survival in

1026   lung adenocarcinoma. *Thorac Cancer* 9: 775-784.

1027   98.   Larroquette, M., J. P. Guegan, B. Besse, S. Cousin, M. Brunet, S. Le Moulec, F. Le

1028   Loarer, C. Rey, J. C. Soria, F. Barlesi, A. Bessede, J. Y. Scoazec, I. Soubeyran, and A.

1029   Italiano. 2022. Spatial transcriptomics of macrophage infiltration in non-small cell lung

1030   cancer reveals determinants of sensitivity and resistance to anti-PD1/PD-L1 antibodies. *J*

1031   *Immunother Cancer* 10.

1032   99.   Zhang, M., W. Yang, P. Wang, Y. Deng, Y. T. Dong, F. F. Liu, R. Huang, P. Zhang, Y.

1033   Q. Duan, X. D. Liu, D. Lin, Q. Chu, and B. Zhong. 2020. CCL7 recruits cDC1 to

promote antitumor immunity and facilitate checkpoint immunotherapy to non-small cell lung cancer. *Nat Commun* 11: 6119.

100. Benci, J. L., L. R. Johnson, R. Choa, Y. Xu, J. Qiu, Z. Zhou, B. Xu, D. Ye, K. L. Nathanson, C. H. June, E. J. Wherry, N. R. Zhang, H. Ishwaran, M. D. Hellmann, J. D. Wolchok, T. Kambayashi, and A. J. Minn. 2019. Opposing Functions of Interferon Coordinate Adaptive and Innate Immune Responses to Cancer Immune Checkpoint Blockade. *Cell* 178: 933-948 e914.

101. Jing, Z. L., G. L. Liu, N. Zhou, D. Y. Xu, N. Feng, Y. Lei, L. L. Ma, M. S. Tang, G. H. Tong, N. Tang, and Y. J. Deng. 2024. Interferon-gamma in the tumor microenvironment promotes the expression of B7H4 in colorectal cancer cells, thereby inhibiting cytotoxic T cells. *Sci Rep* 14: 6053.

102. Zagorulya, M., L. Yim, D. M. Morgan, A. Edwards, E. Torres-Mejia, N. Momin, C. V. McCreery, I. L. Zamora, B. L. Horton, J. G. Fox, K. D. Wittrup, J. C. Love, and S. Spranger. 2023. Tissue-specific abundance of interferon-gamma drives regulatory T cells to restrain DC1-mediated priming of cytotoxic T cells against lung cancer. *Immunity* 56: 386-405 e310.

103. Quintana, F. J., A. S. Basso, A. H. Iglesias, T. Korn, M. F. Farez, E. Bettelli, M. Caccamo, M. Oukka, and H. L. Weiner. 2008. Control of T(reg) and T(H)17 cell differentiation by the aryl hydrocarbon receptor. *Nature* 453: 65-71.

104. Abron, J. D., N. P. Singh, M. K. Mishra, R. L. Price, M. Nagarkatti, P. S. Nagarkatti, and U. P. Singh. 2018. An endogenous aryl hydrocarbon receptor (AhR) ligand, ITE induces regulatory T cells (Tregs) and ameliorates experimental colitis. *Am J Physiol Gastrointest Liver Physiol*.

105. Apetoh, L., F. J. Quintana, C. Pot, N. Joller, S. Xiao, D. Kumar, E. J. Burns, D. H. Sherr, H. L. Weiner, and V. K. Kuchroo. 2010. The aryl hydrocarbon receptor interacts with c-Maf to promote the differentiation of type 1 regulatory T cells induced by IL-27. *Nat Immunol* 11: 854-861.

106. Quintana, F. J., G. Murugaiyan, M. F. Farez, M. Mitsdoerffer, A. M. Tukpah, E. J. Burns, and H. L. Weiner. 2010. An endogenous aryl hydrocarbon receptor ligand acts on dendritic cells and T cells to suppress experimental autoimmune encephalomyelitis. *Proc Natl Acad Sci U S A*.

107. Neamah, W. H., N. P. Singh, H. Alghetaa, O. A. Abdulla, S. Chatterjee, P. B. Busbee, M. Nagarkatti, and P. Nagarkatti. 2019. AhR activation leads to massive mobilization of myeloid-derived suppressor cells with immunosuppressive activity through regulation of CXCR2 and microRNA miR-150-5p and miR-543-3p that target anti-inflammatory genes. *J Immunol* 203: 1830-1844.

108. Liu, K., J. Huang, J. Liu, C. Li, G. Kroemer, D. Tang, and R. Kang. 2022. HSP90 Mediates IFNgamma-Induced Adaptive Resistance to Anti-PD-1 Immunotherapy. *Cancer Res* 82: 2003-2018.

109. Ivashkiv, L. B. 2018. IFNgamma: signalling, epigenetics and roles in immunity, metabolism, disease and cancer immunotherapy. *Nat Rev Immunol* 18: 545-558.

110. Ramana, C. V., M. P. Gil, Y. Han, R. M. Ransohoff, R. D. Schreiber, and G. R. Stark. 2001. Stat1-independent regulation of gene expression in response to IFN-gamma. *Proc Natl Acad Sci U S A* 98: 6674-6679.

111. Pfeffer, L. M. 2011. The role of nuclear factor kappaB in the interferon response. *J Interferon Cytokine Res* 31: 553-559.

112. Kim, D. W., L. Gazourian, S. A. Quadri, R. Romieu-Mourez, D. H. Sherr, and G. E. Sonenshein. 2000. The RelA NF-kB subunit and the aryl hydrocarbon receptor (AhR) cooperate to transactivate the c-myc promoter in mammary cells   *Equal contributions. *Oncogene* 19: 5498-5506.

113. Vogel, C. F., E. Sciullo, W. Li, P. Wong, G. Lazennec, and F. Matsumura. 2007. RelB, a New Partner of Aryl Hydrocarbon Receptor-Mediated Transcription. *Mol Endocrinol* 21: 2941-2955.

114. Inozume, T., K. Hanada, Q. J. Wang, M. Ahmadzadeh, J. R. Wunderlich, S. A. Rosenberg, and J. C. Yang. 2010. Selection of CD8+PD-1+ lymphocytes in fresh human melanomas enriches for tumor-reactive T cells. *J Immunother* 33: 956-964.

115. Simon, S., V. Vignard, L. Florenceau, B. Dreno, A. Khammari, F. Lang, and N. Labarriere. 2016. PD-1 expression conditions T cell avidity within an antigen-specific repertoire. *Oncoimmunology* 5: e1104448.

116. Gros, A., M. R. Parkhurst, E. Tran, A. Pasetto, P. F. Robbins, S. Ilyas, T. D. Prickett, J. J. Gartner, J. S. Crystal, I. M. Roberts, K. Trebska-McGowan, J. R. Wunderlich, J. C. Yang, and S. A. Rosenberg. 2016. Prospective identification of neoantigen-specific lymphocytes in the peripheral blood of melanoma patients. *Nat Med* 22: 433-438.

Footnotes

[*]Graduate Program in Genetics and Genomics, Boston University School of Medicine

[#]Department of Environmental Health, Boston University School of Public Health

[##]Section of Computational Biomedicine, Boston University Chobanian & Avedisian School of Medicine

Abbreviations: Aryl Hydrocarbon Receptor (AhR); B(a)P, Benzo(a)pyrene; DGE, Differentially gene expression; DEG, Differentially expressed gene(s); FICZ, 6-formylindolo(3,2-b)carbazole; GSVA, Geneset variation analysis; GSEA, Gene Set Enrichment Analysis; LUAD, Kyn, Kynurenine; Lung adenocarcinoma; NSCLC, Non-small Cell Lung Cancer; TME, scRNA-seq, single cell RNA sequencing; TCDD, 2,3,7,8-tetrachlorodibenzo-p-dioxin Tumor Microenvironment.

Figure and Table Legends

Figure 1. Bulk RNA-seq analysis of AhR-knockout murine and human lung adenocarcinoma cell lines. RNA was extracted from three sets of CMT167^{Cas9} control, CMT167^{AhR-KO}, A549^{Cas9} control, or A549^{AhR-KO} cells, reversed transcribed, and cDNA sequenced using the Illumina NextSeq 2000 platform. Data are presented as counts defined as the number of read pairs aligning uniquely to the genome in proper pairs and assigned to a single Ensembl Gene locus for each gene transcript. **A)** Heatmap of all genes with 2-fold or greater change in expression with a false discovery rate (FDR) <0.05 after AhR knockout, as comparison with Cas9 controls, in CMT167 (left) or A549 (right) cells. **B)** Representative cancer- or immune-related genes found to be highly differently downregulated upon AhR knockout in CMT167 and A549 cells.

Figure 2. AhR knockout reduces expression of several LUAD-associated genes. Eight genes associated with LUAD and downregulated in CMT167^{AhR-KO}, as indicated by RNA-seq (**Fig. 1**), were quantified by RT-qPCR. There were no statistical differences here or elsewhere between gene levels in AhR^{WT} or AhR^{Cas9} cells. Therefore, results from those two control lines were pooled and referred to here and elsewhere as "Ctrl". Data are presented as means + SE from three independent experiments with duplicates. in each *p<0.05, **p<0.01, ***p<0.001, ****p<0.0001 (Student's t-test, equal variance).

Figure 3. B(a)P, a cigarette smoke constituent, induces PD-L1 and IDO in murine CMT167 cells. A) Expression of *Cd274*, *Ido1*, *Ido2*, *Cyp1a1*, and *Cyp1b1* mRNA was quantified by RT-qPCR in control and CMT167^{AhR-KO} cells (left two bars in each plot) or after 72 hours of treatment with 10 μM benzo(a)pyrene (B(a)P)(right two bars in each plot). Data from three independent experiments, each in duplicate or triplicate are presented as *Gapdh*-normalized

1135   means + SE. **B)** Protein extracted from cells treated as in (**A**) was probed by western

1136   immunoblotting for PD-L1 and, as a loading control, β-actin. One of three representative western

1137   blots is shown on the left and β-actin-normalized protein band densities are on the right. Band

1138   density data are presented as means from three experiments, each in triplicate, + SE. **C)** The

1139   percentage of Kyn$^+$ CMT167^{WT} or CMT167^{AhR-KO} cells treated with vehicle or B(a)P as in (**A**)

1140   was quantified by flow cytometry. Data from two experiments, each in triplicate, are presented

1141   as means + SE from. *p<0.05, **p<0.01, ****p<0.0001 (Student's t-test, equal variance).

1142   **Figure 4. The AhR mediates IFNγ induction of immune-related genes *Cd274, Ido1/2, Jak2,***

1143   **and *Stat1* in murine LUAD CMT167 cells. A)** CMT167^{Ctrl} or CMT167^{AhR-KO} cells were

1144   untreated or treated with 100 ng/ml IFNγ. *Cd274* mRNA was quantified by RT-qPCR 24h later.

1145   *Ido1*, *Ido2*, *Cyp1a1*, and *Cyp1b1* mRNA was quantified 72h later. Data are from three

1146   independent experiments, each in duplicate or triplicate, are expressed as fold change of *Gapdh*-

1147   normalized means + SE. **B)** CMT167^{Ctrl} or CMT167^{AhR-KO} cells were left untreated or treated for

1148   24h with 100 ng/ml IFNγ and PD-L1 protein expression assayed by western immunoblotting. A

1149   representative immunoblot is on the left and β-actin normalized band densities, averaged from

1150   three independent experiments, is on the right. (Bands from IFNγ-treated cells reached saturation

1151   prior to bands from untreated cells becoming visible). **C)** CMT167^{Ctrl} or CMT167^{AhR-KO} cells

1152   were treated for 24h with IFNγ and IDO1 protein expression assayed by western

1153   immunoblotting. A representative immunoblot is on the left and β-actin normalized band

1154   densities, averaged from three independent experiments, are on the right. **D)** CMT167^{Ctrl} or

1155   CMT167^{AhR-KO} cells were treated with 1-1000 ng/ml IFNγ for 24h and Kyn released into the

1156   media quantified via colorimetric assay. Data are averaged from two independent experiments

1157   each in quadruplicate + SE. **E)** CMT167^{Ctrl} or CMT167^{AhR-KO} cells were treated with 100 ng/ml

1158   IFNγ and *Jak2* and *Stat1* mRNA quantified 24h later. RT-qPCR data are from three independent

1159   experiments, each in triplicate, and presented as *Gapdh*-normalized means + SE. *p<0.05,

1160   **p<0.01, ***p<0.001, ****p<0.0001 (Student's t-test, equal variance).

1161   **Figure 5. The AhR mediates IFNγ induction of immune-related genes *CD274, IDO1, JAK2,***

1162   ***STAT1*, and *STAT3* in human LUAD A549 cells. A)** A549^{Ctrl} or A549^{AhR-KO} cells were

1163   untreated or treated with 100 ng/ml IFNγ for 24h and *CD274*, *IDO1,* and *CYP1B1* expression

1164   quantified by RT-qPCR. Data from four experiments, each in triplicate, are represented as fold

1165   change of *GAPDH*-normalized means + SE. **B)** The percent positive PD-L1$^+$ cells treated as in

1166   (**A**) was quantified by flow cytometry. Data from three experiments, each in triplicate, are

1167   presented as mean percent PD-L1$^+$ + SE. **C)** The baseline percent of Kyn$^+$ A549^{ctrl} and A549^{AhR-}

1168 ^{KO} cells in two experiments, each in triplicate, was determined by flow cytometry. **D)** A549^{Ctrl} or

1169   A549^{AhR-KO} cells were treated with 0-1000 ng/ml IFNγ for 24h and Kyn release quantified by the

1170   Kyn-specific colorimetric assay using a standard Kyn curve. Data from two experiments, each in

1171   quadruplicate, are presented as average μM Kyn + SE. **E)** A549^{Ctrl} or A549^{AhR-KO} cells were left

1172   untreated or treated with 100 ng/ml IFNγ for 24h and baseline or 100 ng/ml IFNγ-induced *JAK2,*

1173   *STAT1,* and *STAT3* expression quantified by RT-qPCR. Data from four experiments, each in

1174   triplicate, are presented as average fold change of *Gapdh*-normalized means + SE. *p<0.05,

1175   **p<0.01, ***p<0.001, ****p<0.0001 (Student's t-test, equal variance).

1176   **Figure 6. AhR deletion in CMT167 cells leads to decreased tumor burden and resistance to**

1177   **re-challenge with wildtype cells**. **A)** 10^6 CMT167^{WT} (black lines), CMT167^{Cas9} (blue lines),

1178   CMT167^{AhR-KO} clone C1 (red lines), or CMT167^{AhR-KO} clone D2 (green lines) cells were injected

1179   subcutaneously into syngeneic C57BL/6 mice and tumor growth determined over a 53-day

1180   period. 100% of mice inoculated with CMT167^{WT} cells grew tumors. No tumors were detected in

1181   49 nine of 64 possible CMT167^{AhR-KO} tumors (77%)(red arrow). **B)** Growth curves of control

1182   (CMT167^{WT} + CMT^{Cas9}, n=32) and CMT167^{AhR-KO} (clones C1+D2, n=15) tumors from "**A**"

1183   were averaged. Data are presented as means $\pm$ SE, m = slopes. p<0.0001 by non-linear best fit

1184   curve comparison.   **C)** Mice that had been inoculated 65 days earlier with CMT167^{AhR-KO} cells

1185   (n=10 CMT167^{AhR-KO} clone C1, n=10 CMT167^{AhR-KO} clone D2) and which had not grown

1186   tumors were re-challenged with CMT167^{WT} cells and tumor growth tracked over 40 days (red

1187   dashed lines). Naïve age-matched mice (n=20) were injected with CMT167^{WT} cells as positive

1188   controls (black lines). 100% of naïve mice inoculated with CMT167^{WT} cells grew tumors. No

1189   tumors were detected in 13 of 20 mice (65%) injected 65 days previously with CMT167^{AhR-KO}

1190   cells (red arrow). **D)** Growth curves of CMT167^{WT} tumors injected in naïve mice or into

1191   previous recipients of CMT167^{AhR-KO} cells were averaged. Data are presented as means + SE.

1192   m=slope by linear regression, p<0.0001.

1193   **Figure 7. CMT167^{AhR-KO} tumors have a higher density of infiltrating CD4$^+$ and CD8$^+$ T**

1194   **cells than CMT167^{WT} tumors.** 10^6 CMT167^{WT} or CMT167^{AhR-KO} cells were injected

1195   subcutaneously into syngeneic C57BL/6 mice. Tumors, if present, were excised between two and

1196   five weeks after cell injection. Approximately half of each five-week tumor was fixed and

1197   sectioned for immunofluorescent studies and the remaining tumor half digested to recover

1198   infiltrating leukocytes. **A)** Representative immunofluorescent images from a total of five

1199   CMT167^{WT} and four CMT167^{AhR-KO} five-week tumors (three sections/tumor) stained with DAPI

1200   (blue), AhR-specific antibody (green), and CD45-specific antibody (red) are shown. **B)** Mean

1201   density (number of cells/tumor mm^2) + SE of CD45$^+$ cells from five CMT167^{WT} and four

1202   CMT167^{AhR-KO} five-week tumors. **C-E)** Tumor infiltrating cells were recovered, counted, and

1203   stained for CD45, CD4, CD8, PD-1, and CD44 and analyzed by flow cytometry. Each dot

55

1204   represents the number of cells/mm^3 (i.e. cell density) from one tumor. Data were obtained from

1205   two to 10 mice per group per week depending on tumors available to excise. *p<0.05, **p<0.01,

1206   ***p<0.001, ****p<0.0001 (Multiple comparisons t tests). **F)**. The percent of all CD4$^+$PD-1$^+$

1207   (left) or CD8$^+$PD-1$^+$ (right) T cells that are also CD44^{high}. Data from two independent

1208   experiments, six mice/condition/experiment, are presented as the percent positive + SE.

1209   **p<0.01, p<0.001 (Student's t-test, equal variance).

1210   **Figure 8**. **scRNA-seq of CD45$^+$ TILs from CMT167^{WT} or CMT167^{AhR-KO} five-week tumors**

1211   **reveals differences in TIL composition. A)** CMT167^{WT} or CMT167^{AhR-KO} tumors excised five

1212   weeks after transplantation as in **Fig. 7** were digested and sorted by flow cytometry for CD45$^+$

1213   cells. RNA from single cells was then sequenced. Greater than 2000 *CD3^{high}* T cells were

1214   recovered from each sample. Sixteen unique CD3 Seurat clusters (#0-15) were identified using

1215   the Immunological Genome Project (ImmGen) reference compendium (43) and the singleR

1216   annotation method. **B)** Clusters were overlayed in green and purple to designate CD4 and CD8

1217   cells respectively. **C,D)** Violin plots identify distinct CD4 (**C**) and CD8 (**D**) T cell populations.

1218   **E)** Clusters were overlayed burnt orange or teal to designate cells from CMT167^{WT} or

1219   CMT167^{AhR-KO} tumors, respectively. The orange polygon indicates the relative transcriptomic

1220   resemblance of clusters 2, 5, 6, 8 from CMT167^{WT} tumors and the teal polygon indicates the

1221   relative transcriptomic similarity of clusters 13 and 14 from CMT^{AhR-KO} tumors. **F)** Proportion

1222   of cells originating from CMT167^{WT} (orange) and CMT167^{AhR-KO} (teal) tumors within each

1223   Seurat cluster. The exact percentage of T cells from CMT167^{WT} tumors is presented at the top.

1224   **Figure 9. Analysis of T cell clusters infiltrating CMT167^{WT} and CMT167^{AhR-KO} tumors. A)**

1225   GSVA enrichment scores of functional capabilities in all CD4 (left) or CD8 (right) T cell clusters

1226   from CMT167^{WT} (orange) and CMT167^{AhR-KO} (teal) tumors. **B) Left:** GSVA enrichment scores
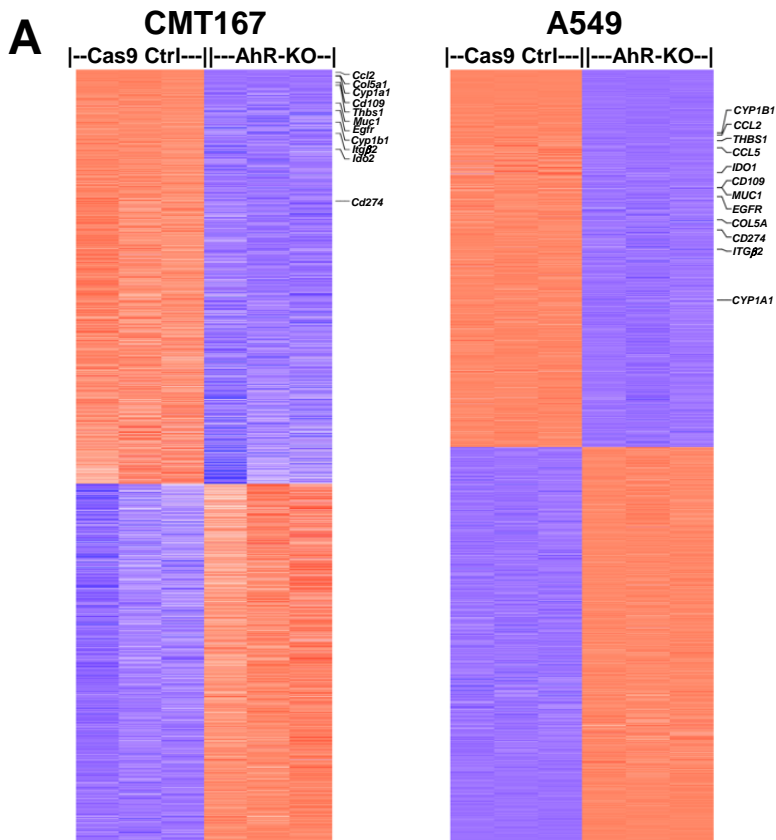
56

1227   of functional capabilities of the aggregate of CMT167^{WT} clusters 2+6+8 vs CMT167^{AhR-KO}

1228   clusters 13+14. **Right:** GSVA enrichment scores of functional capabilities in CMT167^{WT} cluster

1229   6 vs CMT167^{AhR-KO} cluster 13. **C)** The CellChat cell-cell communication platform was used to

1230   predict the number (left) and strength (right) of incoming signals from dendritic cells (DC),

1231   macrophages (MΦ) and B cells to specific CD8 T cell clusters, each of which comprises >90%

1232   of the T cells from the respective CMT167^{WT} or CMT167^{AhR-KO} tumors. The color of the lines

1233   represents the tumor source of T cells (red = CMT167^{AhR-KO}; blue = CMT167^{WT} T cells) and the

1234   thickness represents the relative number or strength of incoming signals from APC. **Top)**

1235   Incoming signals from APC to the aggregate of CMT167^{WT} clusters 2, 6, and 8 versus incoming

1236   signals from APC to the aggregate of CMT167^{AhR-KO} clusters 13 and 14. **Bottom)** Incoming

1237   signals from APC to the CMT167^{WT} clusters 6 versus incoming signals from APC to CMT^{AhR-KO}

1238   cluster 13. **D, E**) MAST (48) was used to analyze immune-related DEGs (p<0.05) between T cell

1239   clusters in which >80% of the cells were derived from CMT167^{WT} or CMT $^{AhR-KO}$ tumors. **D)**

1240   DEGs in CMT167^{WT} CD4 cluster 5 as compared with all other clusters. **E)** DEGs in CMT167^{WT}

1241   CD8 clusters 2,6, and 8 and CMT167^{AhR-KO} clusters 3, 13, and 14 as compared with all other

1242   clusters. The percentage of cells originating from CMT167^{WT} (orange) or CMT^{AhR-KO} (teal)

1243   tumors is restated at the top of the heat maps. **F)** Upregulated genes in CMT167^{AhR-KO} CD8

1244   cluster 13, relative to genes in: 1) all CD8 clusters (left), 2) the aggregate of CMT167^{WT} CD8

1245   clusters 2+6+8 (middle), and 3) CMT167^{WT} CD8 cluster 6 (right) were determined. GSEA was

1246   then used to determine enrichment of these three upregulated cluster 13 gene sets in six sets of

1247   published upregulated genes from: 1) activated CD8 T cells as compared with naïve CD8 T cells

1248   (three gene sets: GSE9650 Eff. vs Naïve CD8 T cells, Goldrath Eff. vs Naïve CD8 T cells,

1249   Kaech Eff. vs Naïve CD8 T cells), 2) activated CD8 T cells as compared with memory CD8 T

1250   cells (two gene sets: GSE9650 Eff. vs Mem. CD8 T cells, Kaech Eff. Vs Mem. CD8 T cells), and

1251   3) activated CD8 T cells as compared with tolerant CD8 T cells (one gene set: GSE14699

1252   Activated vs Tolerant CD8 T cells).

1253   **Figure 10. Working model of IFNγ and AhR-mediated regulation of IDO and PD-L1.** TILs

1254   in the TME generate IFNγ which upregulates AhR activity in malignant cells through an as yet

1255   unidentified pathway(s). AhR signaling boosts the JAK/STAT pathway up-regulating IDO and

1256   PD-L1. IDO contributes to generation of tryptophan-derived AhR ligands including kynurenine

1257   resulting in an AhR amplification loop. Kynurenine and other AhR ligands may activate the AhR

1258   in immune cells in the TME skewing them towards immunosuppressive phenotypes. PD-L1 on
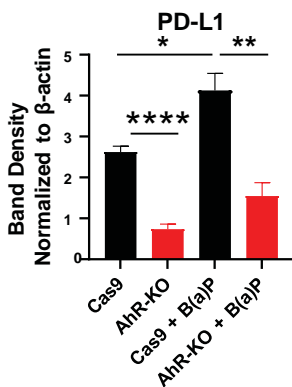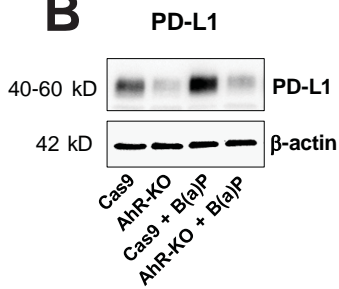
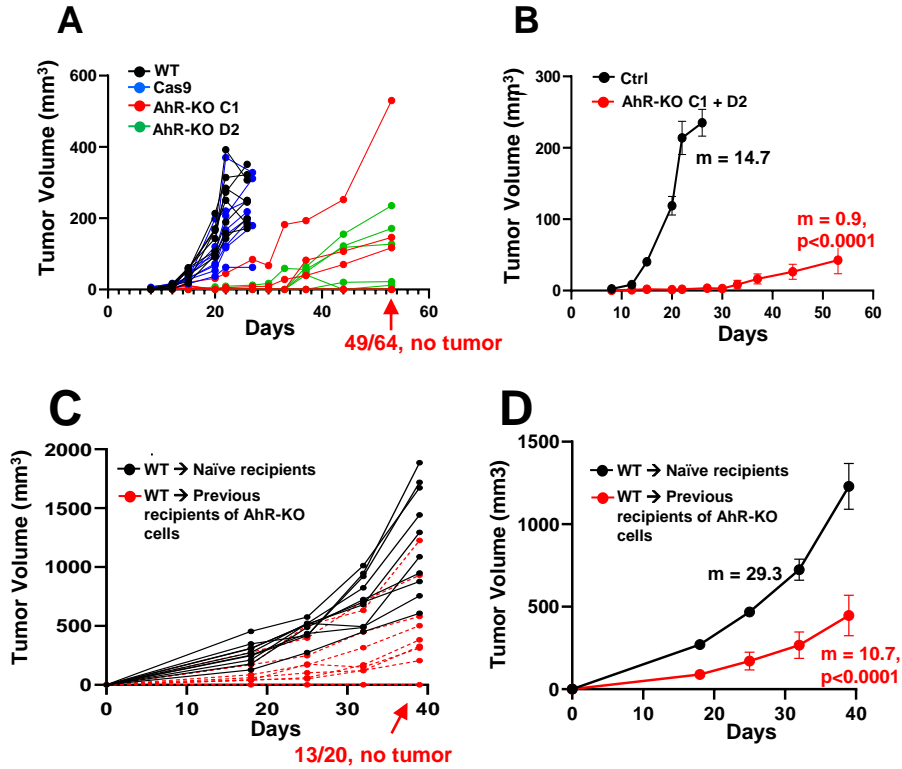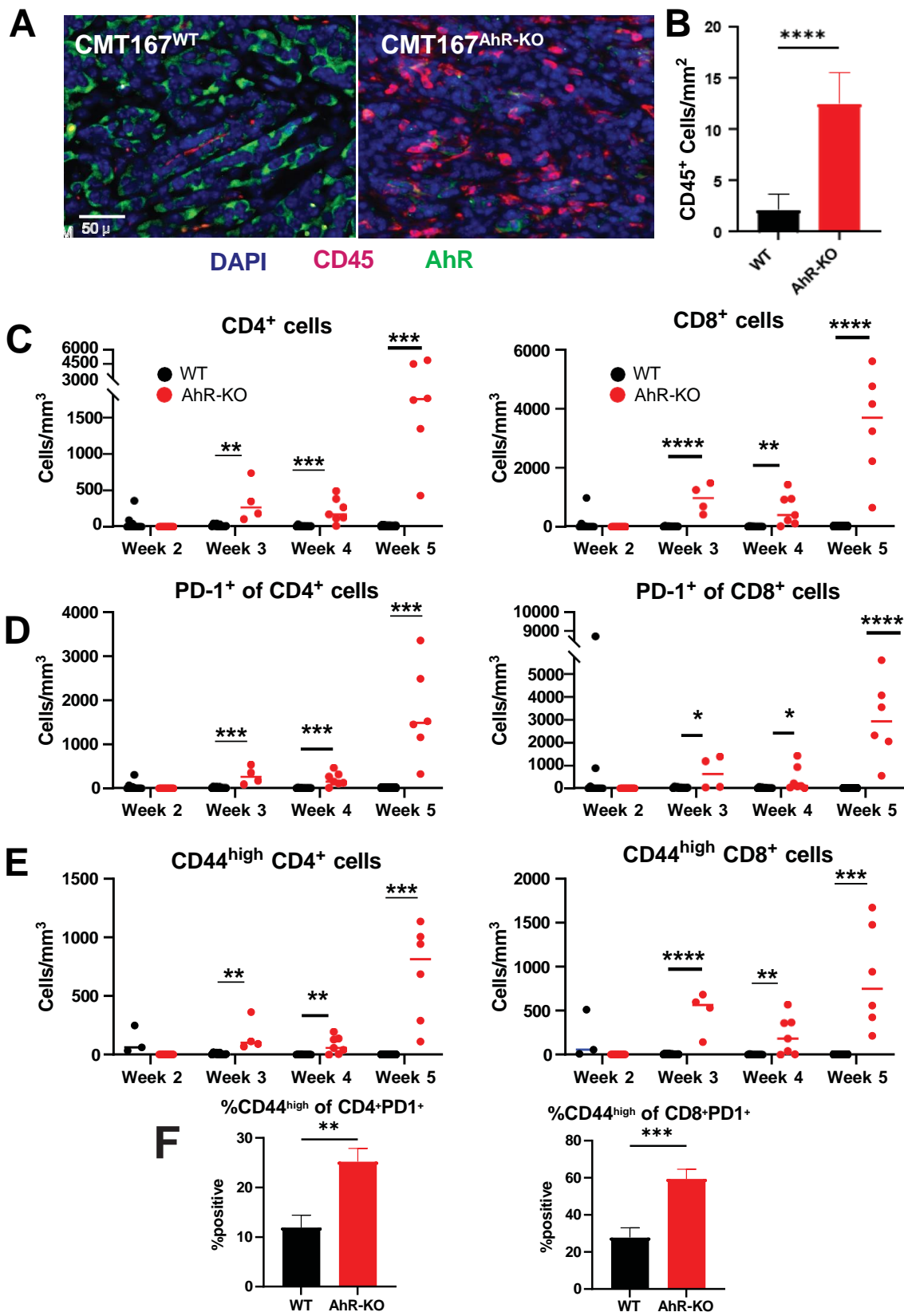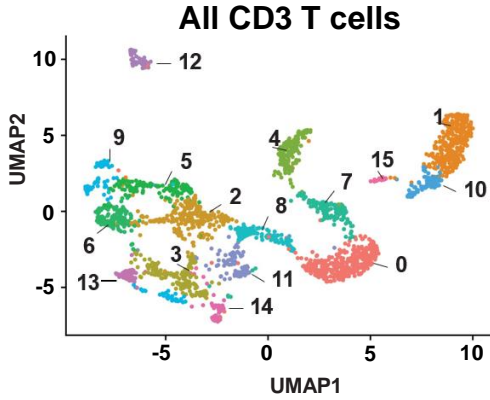1259   malignant cells suppresses immune effector cell function.

Snyder et al. Figure 1

A

CMT167 |--Cas9 Ctrl---||---AhR-KO--|

Labels: Ccl2, Col5a1, Cyp1a1, Cd109, Thbs1, Muc1, Egfr, Cyp1b1, Itgβ2, Ido2, Cd274

A549 |--Cas9 Ctrl---||---AhR-KO--|

Labels: CYP1B1, CCL2, THBS1, CCL5, IDO1, CD109, MUC1, EGFR, COL5A, CD274, ITGβ2, CYP1A1

B

Gene	CMT167		A549	
	Fold Change	FDR q	Fold change	FDR q
CYP1A1	-154.5	$<9 \times 10^{-8}$	-3.7	$<10^{-7}$
CYP1B1	-9.1	$<7 \times 10^{-6}$	-58.3	$<10^{-20}$
MUC1	-22.1	$<10^{-48}$	-16.8	$<4 \times 10^{-60}$
COL5A1	-214.0	$<2 \times 10^{-12}$	-8.9	$<2 \times 10^{-20}$
THBS1	-56.1	$<10^{-50}$	-47.1	$<10^{-20}$
EGFR	-16.2	$<6 \times 10^{-3}$	-13.8	$<10^{-20}$
ITG β2	-6.6	$<6 \times 10^{-3}$	-6	$<5 \times 10^{-45}$
CD109	-68.5	$<2 \times 10^{-5}$	-16.8	$<10^{-20}$
CCL2	-533.6	$<10^{-11}$	-55.8	$<3 \times 10^{-20}$
CCL5	-17.5	$<9 \times 10^{-2}$	-39.9	$<5 \times 10^{-4}$
IDO1	-7.1	<0.5	-23.4	$<3 \times 10^{-2}$
IDO2	-4.4	$<7 \times 10^{-6}$	ND	
CD274	-2.2	$<2 \times 10^{-5}$	-7.7	$<2 \times 10^{-14}$

Snyder et al. Figure 5

Snyder et al. Figure 6

A

Tumor Volume (mm³) vs Days

- WT
- Cas9
- AhR-KO C1
- AhR-KO D2

49/64, no tumor

B

Tumor Volume (mm³) vs Days

- Ctrl
- AhR-KO C1 + D2

m = 14.7

m = 0.9, p<0.0001

C

Tumor Volume (mm³) vs Days

- WT → Naïve recipients
- WT → Previous recipients of AhR-KO cells

13/20, no tumor

D

Tumor Volume (mm3) vs Days

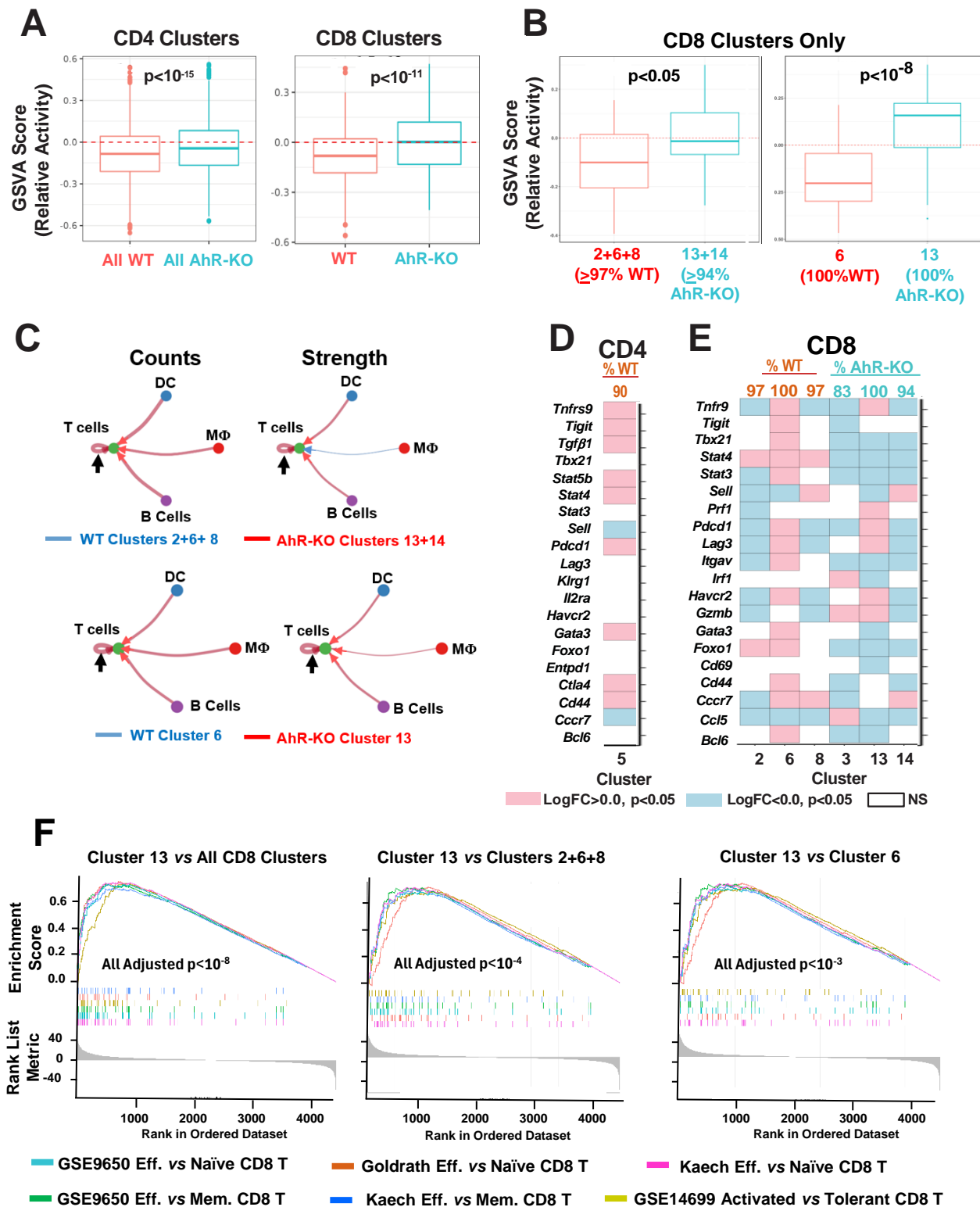- WT → Naïve recipients
- WT → Previous recipients of AhR-KO cells

m = 29.3

m = 10.7, p<0.0001
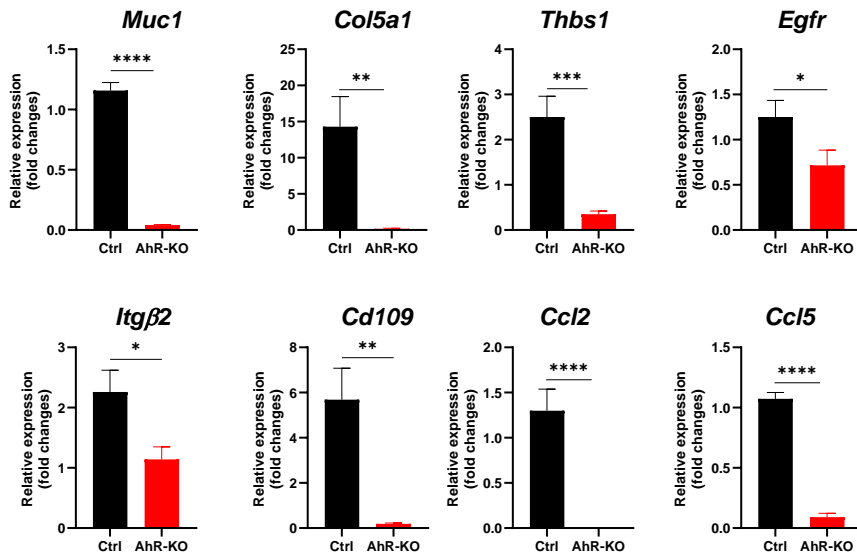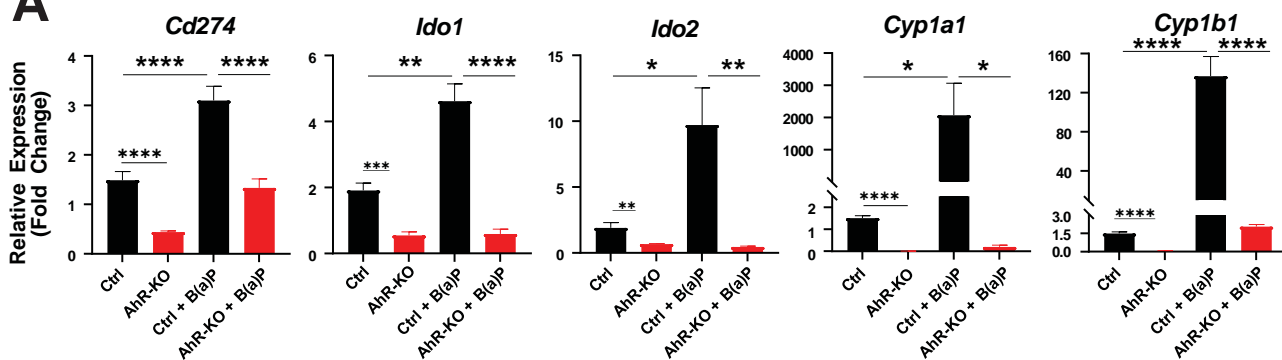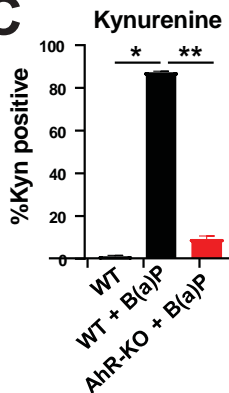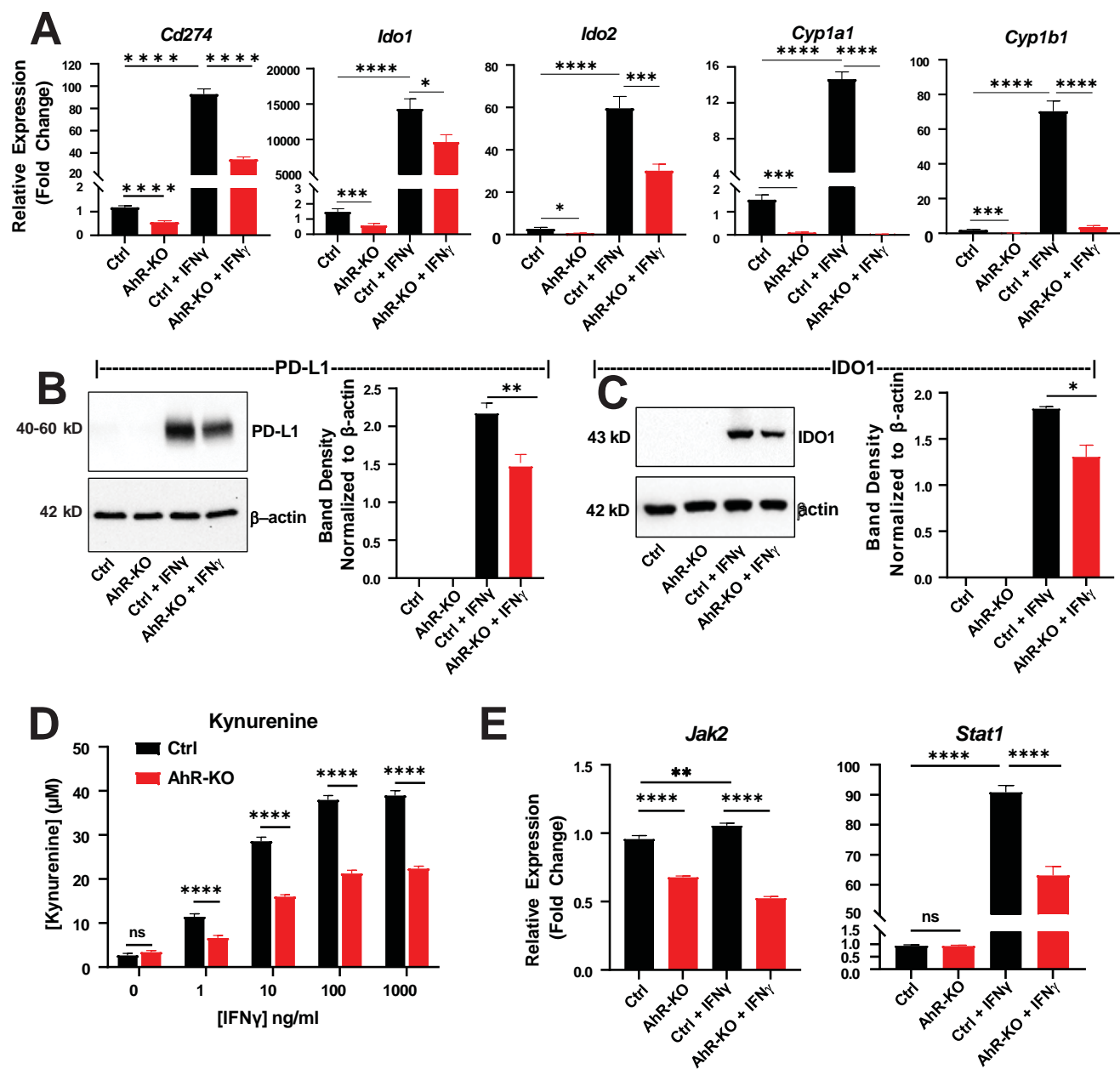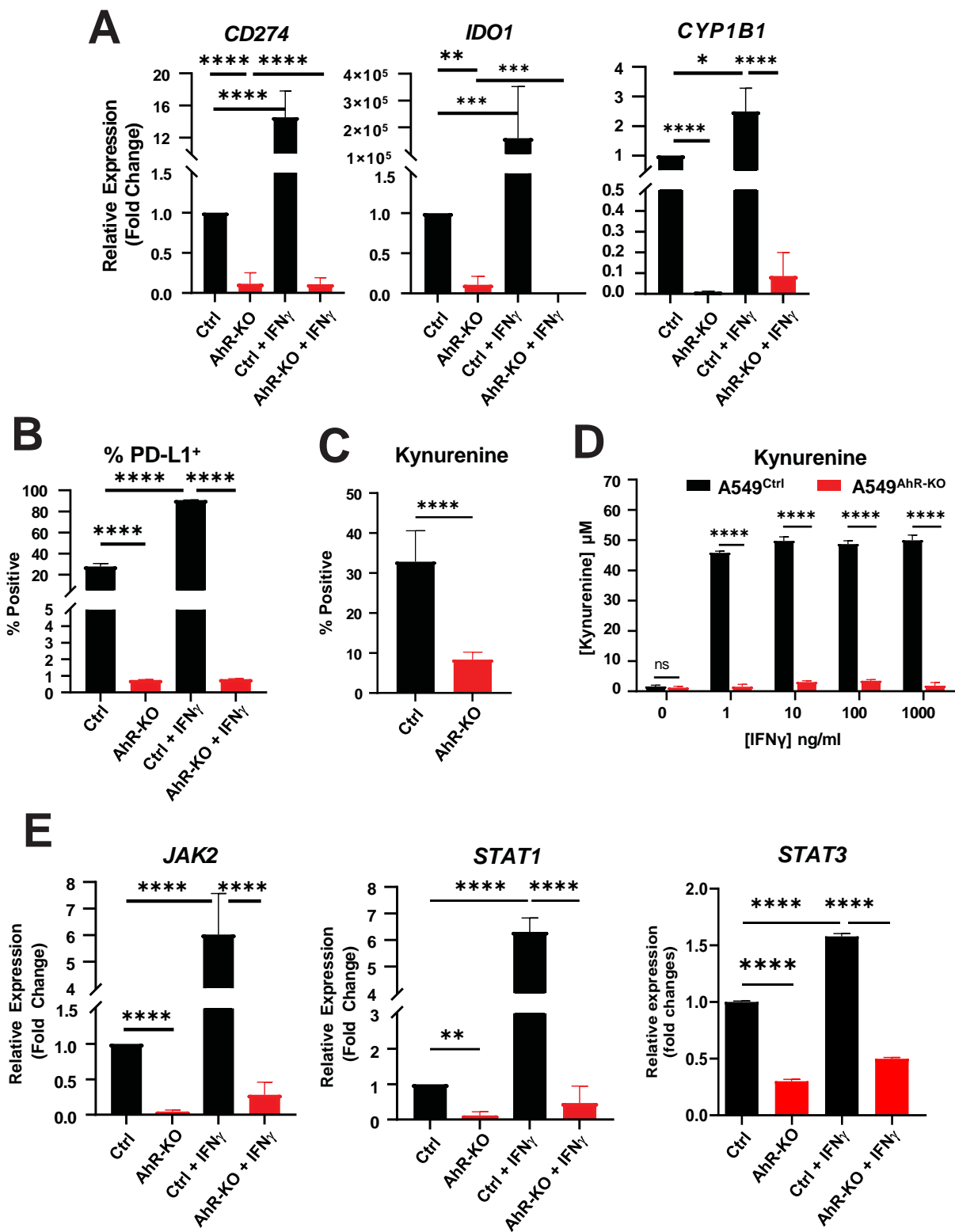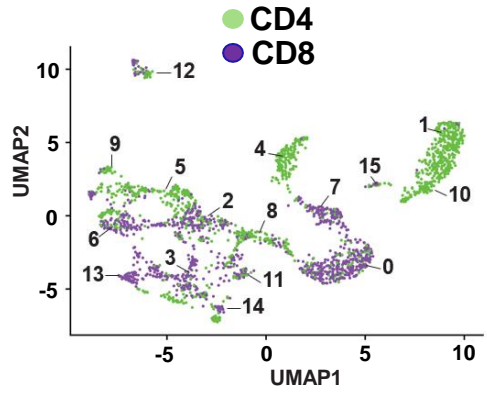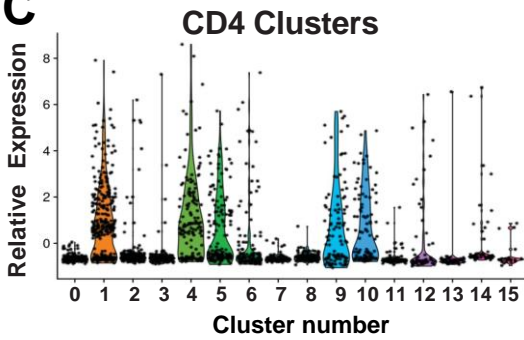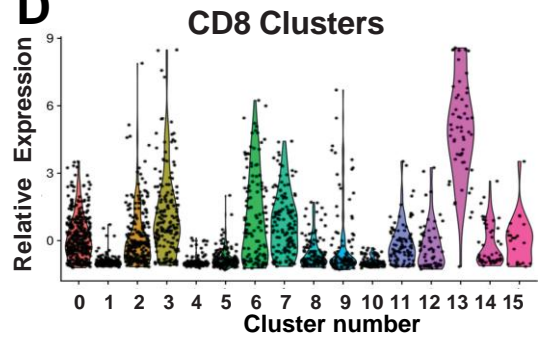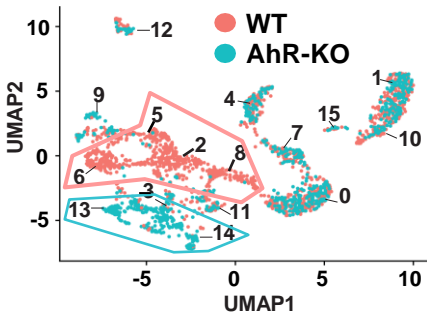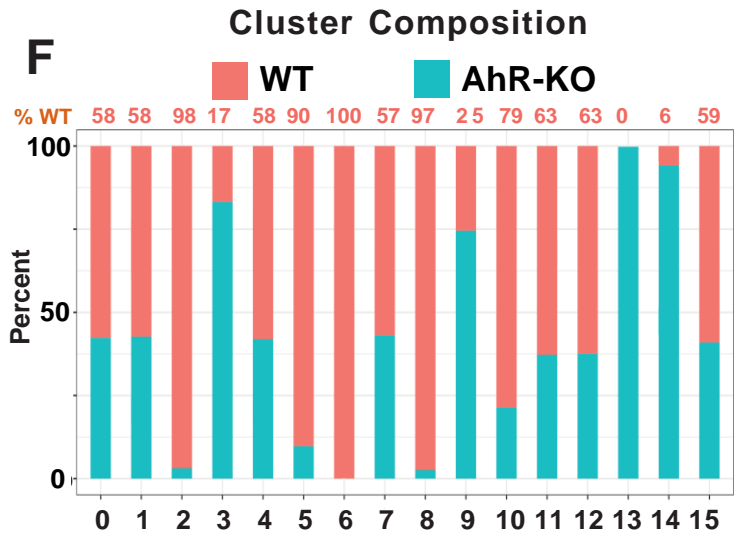
Snyder et al. Figure 9

Snyder et al, Figure 10